NATIONAL ADVISORY COMMITTEE FOR AERONAUTICS

TECHNICAL NOTE 3007

LIFT AND PITCHING MOMENT AT LOW SPEEDS OF THE NACA 64A010 AIRFOIL SECTION EQUIPPED WITH VARIOUS COMBINATIONS OF A LEADING-EDGE SLAT, LEADING-EDGE FLAP, SPLIT FLAP, AND DOUBLE-SLOTTED FLAP

By John A. Kelly and Nora-Lee F. Hayter

Ames Aeronautical Laboratory
Moffett Field, Calif.

Washington
September 1953

lW

NATIONAL ADVISORY COMMITTEE FOR AERONAUT.

TECHNICAL NOTE 3007

LIFT AND PITCHING MOMENT AT LOW SPEEDS OF THE NACA 64A010 AIRFOIL SECTION EQUIPPED WITH VARIOUS COMBINATIONS OF A LEADING-EDGE SLAT, LEADING-EDGE FLAP, SPLIT FLAP, AND DOUBLE-SLOTTED FLAP

By John A. Kelly and Nora-Lee F. Hayter

SUMMARY

A two-dimensional wind-tunnel investigation at low speeds was made of the NACA 64A010 airfoil equipped with various combinations of a leading-edge slat, leading-edge flap, split flap, and double-slotted flap. Optimum slat positions were determined for a Reynolds number of 6 million for the model with no trailing-edge flap and with the two trailing-edge flaps deflected. Section lift and pitching-moment characteristics of the various model arrangements were ascertained for Reynolds numbers of 2, 4, 6, and 7 million.

The increases in the maximum section lift coefficient produced by the leading-edge flap or by the leading-edge slat in combination with either of the trailing-edge flaps were approximately equal to the sum of the increments produced by each of the high-lift devices deflected individually. Extension of the leading-edge slat and deflection of the leading-edge flap produced increments in $c_{l_{max}}$ of about 0.83 and 0.66, respectively. Deflection of either leading-edge high-lift device caused the aerodynamic center to move forward. In the case of the leading-edge slat, the aerodynamic center moved forward to approximately the quarter point of the extended chord.

An empirical method is presented for determining, to a first approximation, the slat position which produces the highest maximum section lift coefficient for a given slat deflection angle.

INTRODUCTION

The design of aircraft for high-speed flight has resulted in the use of swept wings or of straight wings of low aspect ratio with wing thickness of the order of 10-percent chord or less. As a result of the inherently low values of the maximum lift coefficient for such wings, even

when equipped with conventional trailing-edge flaps, increased attention is being given to the use of additional high-lift devices near the leading edge.

An investigation was undertaken to examine the benefits obtainable from a slat or a leading-edge flap combined with trailing-edge flaps on the NACA 64A010 airfoil section. Both the slat and the leading-edge flap were tested on an otherwise plain airfoil model and also in conjunction with either a split flap or a double-slotted flap at the trailing edge. In the course of the investigation, the optimum deflections of the leading-edge flap and optimum positions of the leading-edge slat were determined with the plain airfoil and with both types of trailing-edge flaps.

The tests were conducted in the Ames 7- by 10-foot wind tunnel No. 1 at low speeds and for Reynolds numbers from 2 to 7 million.

NOTATION

c	airfoil chord, ft
c_l	section lift coefficient
$c_{l_{max}}$	maximum section lift coefficient
$\Delta c_{l_{max}}$	increment of maximum section lift coefficient produced by high-lift device
c_m	section pitching-moment coefficient (referred to the quarter-chord point)
R	Reynolds number
t	airfoil thickness, ft
x	distance along chord line, ft
x_s	chordwise displacement of slat reference point in percent of airfoil chord, positive when slat moves forward
Δx	chordwise displacement of leading edge of slat in percent of airfoil chord, positive when slat moves forward
y	distance normal to chord line, ft
y_s	displacement normal to the airfoil chord line of slat reference point in percent of airfoil chord, positive when slat moves upward

Δy	displacement normal to the airfoil chord line of leading edge of slat in percent of airfoil chord, positive when slat moves upward
α	section angle of attack, deg
$\alpha_{c_{l_{max}}}$	section angle of attack corresponding to $c_{l_{max}}$, deg
$\Delta\alpha_{c_{l_{max}}}$	increment of section angle of attack corresponding to $c_{l_{max}}$ produced by high-lift device, deg
δ	angular deflection of high-lift device, deg
χ	distance from slat reference point to trailing edge of slat measured parallel to slat chord line, percent of airfoil chord
τ	distance from slat reference point to trailing edge of slat measured normal to slat chord line, percent of airfoil thickness

Subscripts

n	leading-edge flap
s	leading-edge slat
sf	split flap
dsf	double-slotted flap

MODEL AND TESTS

An NACA 64A010 airfoil with a 5-foot chord was constructed with provision for various combinations of a leading-edge flap or a leading-edge slat with a split flap, or a double-slotted flap. The model spanned what normally would be the 7-foot dimension of the wind tunnel. However, it was found necessary to provide fairings around the brackets that held the upper and lower ends of the slat; therefore, the span was shortened approximately 5 inches by the installation of liners on the tunnel floor and ceiling. The liners extended approximately 4.5 feet upstream of the leading edge and 3.5 feet downstream of the trailing edge of the basic airfoil model.

In the present investigation three model arrangements conformed geometrically to the basic airfoil (ref. 1): the model with the leading-edge flap ($\delta_n = 0^\circ$) and no trailing-edge flap,[1] the model with the slat retracted and no trailing-edge flap,[1] and the model with the slat retracted and the double-slotted flap retracted. Coordinates for the basic airfoil and for the different components of the model are presented in table I. Figure 1 shows sections through the various high-lift devices. The model installed in the wind tunnel is shown by photographs in figure 2. The 60° deflection angle for the split flap and 52.7° for the double-slotted flap were selected because these values are believed to be about optimum for the ratios of flap chord to airfoil chord that were used.

Measurements of lift and pitching moment were made with the wind-tunnel balance system. For the most part, the tests were conducted at a Reynolds number of 6 million. Data also were taken for Reynolds numbers of 2, 4, and 7 million for the basic airfoil model, the model with optimum slat settings, and the model with leading-edge-flap deflections of 10°, 20°, 30°, and 40°. The following table summarizes the conditions for all the tests:

$R \times 10^{-6}$	Dynamic pressure, lb/sq ft	Mach number
2	5	0.06
4	20	.12
6	40	.17
7	60	.20

The data have been corrected for the influence of the tunnel boundaries with the use of the appropriate relations given in reference 2.

To assist in the determination of stalling characteristics, observations were made of the flow over the model as indicated by tufts and by the chordwise distribution of pressure.

RESULTS AND DISCUSSION

Basic Airfoil

Lift and pitching-moment curves for the three models corresponding geometrically to the basic airfoil are presented in figures 3 and 4(a) ($\delta_n = 0^\circ$). The purpose of the following discussion is to point out the changes in $c_{l_{max}}$ that resulted from replacing the leading-edge flap with the slat and from alteration of the trailing-edge region to

[1]Before adaptation for the double-slotted flap.

accommodate the double-slotted flap. The data from figure 3(b) ($R = 6 \times 10^6$) and figure 4(a) ($\delta_n = 0^\circ$) show that $c_{l_{max}}$ was 0.90 for the model with the slat retracted and no trailing-edge flap and 1.10 for the model with the leading-edge flap undeflected and no trailing-edge flap. The possible effects of leakage around the slat were investigated by sealing the upper and lower surface slat-wing junctures. A comparison of the results for the model in the sealed and unsealed conditions showed no changes in the lift or pitching moment. The effect of revising the trailing-edge region to permit the installation of the double-slotted flap was to increase $c_{l_{max}}$ from 0.90 to 1.03 (fig. 3(b), $R = 6 \times 10^6$). Similar increases were obtained for the other values of Reynolds number. Data for the model with the leading-edge flap ($\delta_n = 0^\circ$) and no trailing-edge flap will be considered as the basic airfoil data for this report since they correspond most nearly to the data from reference 1. With either type of trailing-edge flap deflected there was little or no difference in the value of $c_{l_{max}}$ for the model with the slat retracted or with the leading-edge flap undeflected.

Leading-Edge Flap

The data presented in figure 5 show the effect of varying the deflection of the leading-edge flap on the maximum lift coefficient for the model with different trailing-edge-flap arrangements. The maximum lift coefficient was increased by increasing the leading-edge-flap deflection up to an angle which was dependent on the Reynolds number. For a Reynolds number of 2×10^6, the curves reach their peak values for a deflection angle of approximately 40°. For the higher Reynolds numbers, the peak values were reached at approximately 30° deflection. The absence of data for leading-edge-flap angles between 0° and 40° for the model with a split flap at a Reynolds number of 7×10^6 is due to having stopped these runs prior to attaining $c_{l_{max}}$ because of extremely violent shaking of the model. The dashed curve was drawn through values obtained for $\delta_n = 0^\circ$ and 40° and from increments of $c_{l_{max}}$, produced by the trailing-edge flap, extrapolated to a Reynolds number of 7×10^6.

In figure 4 are shown the lift and pitching-moment characteristics of the model for various deflections of the leading-edge flap. The linear portion of the lift curve for the model with a trailing-edge flap was decreased considerably by increasing the leading-edge-flap deflection beyond 30°.

The stalling characteristics of the various model arrangements as indicated from observations of tufts and pressure distributions are classified in accordance with the types described in reference 3. The type of stall associated with the plain NACA 64A010 airfoil section — leading-edge stall (abrupt flow separation near the leading edge without subsequent

reattachment) — was not altered by deflection of the leading-edge flap for the model with no trailing-edge flap. However, the chord-wise location of the point of flow separation which was near the leading edge of the leading-edge flap for deflections up to 15°, moved downstream of the leading-edge flap for deflections greater than 15°. Deflection of the split flap for the model with $\delta_n = 0°$ resulted in a change to the thin-airfoil type of stall (flow separation at the leading edge, prior to attaining $c_{l_{max}}$, with reattachment at a point which moves progressively rearward with increasing angle of attack), but leading-edge-flap deflections of 5° or greater caused the stall to revert to the leading-edge type. Deflection of the double-slotted flap resulted in a trailing-edge stall wherein the attainment of $c_{l_{max}}$ corresponded to the flow separation having progressed forward to approximately the 60-percent-chord station, regardless of the amount of leading-edge-flap deflection.

Leading-Edge Slat

Determination of optimum slat positions.- The effect of slat position on the maximum section lift coefficient is shown by the contours in figures 6, 7, and 8. The highest values of the maximum section lift coefficient are plotted against slat deflection in figure 9. The positions corresponding to the peak values shown in figure 9 will be referred to hereinafter as optimum positions. Reference dimensions for these various positions are given in the following table:

Slat in optimum position for the model with -	x_s, percent chord	y_s, percent chord	Gap, percent chord	δ_s, deg
No trailing-edge flap	9.2	-8.7	1.60	25.6
Split flap deflected 60°	8.2	-9.3	1.25	29.1
Double-slotted flap deflected 52.7°	7.9	-8.1	1.10	26.1

The changes in optimum slat position due to deflection of the split flap are consistent with the trends noted in reference 4. Deflection of the trailing-edge high-lift devices caused the optimum slat position to be changed in such a manner as to reduce the gap.

In an attempt to obtain some criteria for the positioning of a leading-edge slat to attain high values of maximum lift, data corresponding to the highest values of $c_{l_{max}}$ from the contour plots of

references 4 and 5 and from the present report were correlated. The results are presented in figure 10. The graph of $(\Delta x/\chi)$ as a function of gap/τ indicates that, if the relation of Δx to the gap is adjusted for the geometry of the concave surface of the slat, there is but a single value of Δx for a given gap which will produce the highest $c_{l_{max}}$ for a particular slat deflection.

The contour plots from the present report and reference 4 were used to check the reliability of the curves drawn in the graphs of $-(\Delta y/\Delta x)$ vs. δ_s and $(\Delta x/\chi)$ vs. gap/τ. The point of intersection of lines determined from these two curves was located on the appropriate contour plot, and the loss in $c_{l_{max}}$ from the highest value shown on the plot was ascertained. The errors in estimating $c_{l_{max}}$ are plotted for the corresponding values of δ_s and show that, generally, the errors are less than 0.1 and have an average value of approximately 0.05. Therefore, it is felt that the curves in the graphs of $-(\Delta y/\Delta x)$ vs. δ_s and $(\Delta x/\chi)$ vs. gap/τ would provide a good first approximation in determining a slat position that would result in attaining the highest value of $c_{l_{max}}$ for a given slat deflection.

To apply the data of figure 10 to a proposed slat installation, first select a value for δ_s.[2] Then, lay out the contour of the airfoil with the slat retracted and through the leading edge draw a line with a slope equal to the value of $-(\Delta y/\Delta x)$ (corresponding to the selected δ_s) determined from the graph of $-(\Delta y/\Delta x)$ vs. δ_s. Move the proposed slat, deflected δ_s°, along this line until the values of the gap and Δx combine to give a point on the curve in the graph of $(\Delta x/\chi)$ vs. gap/τ.

Aerodynamic characteristics with the slat extended.- The lift and pitching-moment characteristics of the model with the slat in each of the three optimum positions described previously are presented in figures 11, 12, and 13 for four values of Reynolds numbers. For a Reynolds number of 6×10^6 the highest value of $c_{l_{max}}$ obtained for the model without a flap was 1.94 (fig. 11(b)); with the split flap deflected, 2.81 (fig. 12(b)); and with the double-slotted flap deflected, 3.08 (fig. 13(b)). The value 3.08 was the highest value of $c_{l_{max}}$ obtained during the slat investigation and was approximately the same as the highest value of $c_{l_{max}}$ obtained for the model with the combination of leading-edge flap and double-slotted flap deflected.

In general, $c_{l_{max}}$ increased as the Reynolds number was increased from 2×10^6 to 6×10^6 and then decreased for 7×10^6. It is not clear

[2]The values of δ_s that would result in an optimum position are generally much higher than the values used in current slat installations on actual airplanes. This is due to the limitations on the angular deflection imposed by mechanical linkage and/or structural considerations for the airplane.

whether the decrease in $c_{l_{max}}$ for $R = 7 \times 10^6$ was an effect of Reynolds number or of Mach number since these parameters were not varied independently. References 6 and 7 show evidence that $c_{l_{max}}$ for airfoils with large amounts of camber near the leading edge can be expected to decrease with increasing Reynolds number. On the other hand, reference 8 states that for Mach numbers of the order of 0.2, increasing Mach number can bring about flow separation and losses in $c_{l_{max}}$. Therefore, either or both effects may have influenced the results of the present investigation.

Extension of the slat caused the stall for the models to be of the trailing-edge type (ref. 3). The lift curves in figure 11 for a Reynolds number of 4×10^6 can be used to illustrate some of the differences in the stalling characteristics. Data for the model without a flap, for which there was a rounding of the lift curve above an angle of attack of approximately 16° show that a large region of separated flow (approximately 55-percent chord) was present when $c_{l_{max}}$ was reached. The point of separation moved forward slowly and caused no abrupt losses in lift when the angle of attack for $c_{l_{max}}$ had been exceeded. A somewhat smaller region of separated flow (approximately 35-percent chord) was present in the case of the model with either of the flaps deflected, and there was less rounding of the lift curves near the peaks. However, the forward progression of the point of separation was more rapid for the model with the split flap than for the model with the double-slotted flap, and there was a sudden loss of lift once $c_{l_{max}}$ had been reached.

The effects of extension of the slat on the pitching-moment characteristics may be shown by comparing the pitching-moment curves from figure 3 with corresponding curves from figure 11, 12, or 13. Regardless of which optimum slat position or trailing-edge-flap arrangement is considered, extension of the slat caused the aerodynamic center to move forward to approximately the quarter point of the extended chord.

A summary of the maximum-lift data for the various models is contained in table II.

CONCLUSIONS

Results of a two-dimensional wind-tunnel investigation of an NACA 64A010 airfoil equipped with a leading-edge flap, a leading-edge slat, a split flap, and a double-slotted flap indicate the following conclusions:

1. The increases in the maximum section lift coefficient produced by the leading-edge flap or the leading-edge slat in combination with either of the trailing-edge flaps were approximately equal to the sum of the increments produced by each of the high-lift devices deflected

individually. The average increment in $c_{l_{max}}$ was 0.83 for the leading-edge slat and 0.66 for the leading-edge flap.

2. Deflection of either leading-edge high-lift device caused the aerodynamic center to move forward. In the case of the leading-edge slat, the aerodynamic center moved forward to approximately the quarter point of the extended chord.

3. Deflection of the trailing-edge high-lift devices caused the optimum slat position to be changed in such a manner as to reduce the gap.

4. For all trailing-edge arrangements, the deflection angle of the leading-edge flap giving the highest value of $c_{l_{max}}$ decreased from 40° for a Reynolds number of 2 million to 30° for Reynolds numbers of 4, 6, and 7 million.

Ames Aeronautical Laboratory
National Advisory Committee for Aeronautics
Moffett Field, Calif., June 25, 1953.

REFERENCES

1. Loftin, Laurence K., Jr.: Theoretical and Experimental Data for a Number of NACA 6A-Series Airfoil Sections. NACA Rep. 903, 1948.

2. Allen, H. Julian, and Vincenti, Walter G.: Wall Interference in a Two-Dimensional-Flow Wind Tunnel, with Consideration of the Effect of Compressibility. NACA Rep. 782, 1944.

3. McCullough, George B., and Gault, Donald E.: Examples of Three Representative Types of Airfoil-Section Stall at Low Speed. NACA TN 2502, 1951.

4. Gottlieb, Stanley M.: Two-Dimensional Wind-Tunnel Investigation of Two NACA 6-Series Airfoils with Leading-Edge Slats. NACA RM L8K22, 1949.

5. Schuldenfrei, Marvin J.: Wind-Tunnel Investigation of an NACA 23012 Airfoil with a Handley Page Slat and Two Flap Arrangements. NACA WR L-261, 1942. (Formerly NACA ARR, Feb. 1942)

6. Jacobs, Eastman N., and Sherman, Albert: Airfoil Section Characteristics as Affected by Variations of the Reynolds Number. NACA Rep. 586, 1937.

7. Jacobs, Eastman N., Pinkerton, Robert M., and Greenberg, Harry: Tests of Related Forward-Camber Airfoils in the Variable-Density Wind Tunnel. NACA Rep. 610, 1937.

8. Stack, John: Compressibility Effects in Aeronautical Engineering. NACA ACR, 1941.

TABLE I.- COORDINATES OF NACA 64A010 AIRFOIL, LEADING-EDGE SLAT, AND DOUBLE-SLOTTED FLAP

[Stations and ordinates given in percent of airfoil chord]

(a) NACA 64A010 Airfoil

Upper surface		Lower surface	
Station	Ordinate	Station	Ordinate
0	0	0	0
.5	.804	.5	-.804
.75	.969	.75	-.969
1.25	1.225	1.25	-1.225
2.5	1.688	2.5	-1.688
5.0	2.327	5.0	-2.327
7.5	2.805	7.5	-2.805
10.0	3.199	10.0	-3.199
15.0	3.813	15.0	-3.813
20.0	4.272	20.0	-4.272
25.0	4.606	25.0	-4.606
30.0	4.837	30.0	-4.837
35.0	4.968	35.0	-4.968
40.0	4.995	40.0	-4.995
45.0	4.894	45.0	-4.894
50.0	4.684	50.0	-4.684
55.0	4.388	55.0	-4.388
60.0	4.021	60.0	-4.021
65.0	3.597	65.0	-3.597
70.0	3.127	70.0	-3.127
75.0	2.623	75.0	-2.623
80.0	2.103	80.0	-2.103
85.0	1.582	85.0	-1.582
90.0	1.062	90.0	-1.062
95.0	.541	95.0	-.541
100.0	.021	100.0	-.021
L.E. radius: 0.687			
T.E. radius: 0.023			

TABLE I.- COORDINATES OF NACA 64A010 AIRFOIL, LEADING-EDGE SLAT, AND DOUBLE-SLOTTED FLAP - Continued

[Stations and ordinates given in percent of airfoil chord]

(b) Leading-Edge Slat

Slat lower surface		Upper surface of airfoil	
Station	Ordinate	Station	Ordinate
4.7	-2.200	4.9	-2.256
4.8	-1.852	5.0	-1.874
5.0	-1.364	5.2	-1.347
5.2	-.992	5.4	-.983
5.4	-.687	5.6	-.694
5.7	-.322	5.8	-.451
6.0	-.032	6.0	-.240
6.5	.395	6.5	.204
7.0	.745	7.0	.576
7.5	1.047	7.5	.908
8.0	1.307	8.0	1.193
9.0	1.746	9.0	1.655
10.0	2.113	10.0	2.034
11.0	2.433	11.0	2.361
12.0	2.712	12.0	2.652
13.0	2.969	13.0	2.921
14.0	3.216	14.0	3.176
15.0	3.459	15.0	3.434
16.0	3.703	16.0	3.691
17.0	3.948	17.0	3.948

TABLE I.- COCRDINATES OF NACA 64A010 AIRFOIL, LEADING-EDGE SLAT, AND DOUBLE-SLOTTED FLAP - Continued

[Stations and ordinates given from airfoil chord line in percent of airfoil chord]

(c) Double-Slotted Flap, Main Flap

Upper surface		Lower surface	
Station	Ordinate	Station	Ordinate
75.000	-1.000	75.000	-1.000
75.150	-.371	75.150	-1.557
75.295	-.076	75.295	-1.712
75.587	.286	75.587	-1.956
75.882	.535	75.882	-2.095
76.177	.751	76.177	-2.179
76.765	1.057	76.765	-2.289
77.352	1.272	77.352	-2.320
77.942	1.414	77.942	-2.304
78.530	1.496	78.530	-2.260
79.705	1.594	79.705	-2.136
80.882	1.637	80.882	-2.003
82.060	1.648	82.060	-1.880
83.235	1.630	83.235	-1.762
84.410	1.583	84.410	-1.641
85.000	1.550	85.000	-1.582
86.250	1.453	86.250	-1.453
90.000	1.062	90.000	-1.062
95.000	.541	95.000	-.541
100.000	.021	100.000	-.021
L.E. radius: 0.95 (center on main flap chord line)			
T.E. radius: 0.023			

TABLE I.- COORDINATES OF NACA 64A010 AIRFOIL, LEADING-EDGE SLAT, AND DOUBLE-SLOTTED FLAP - Concluded

[Stations and ordinates given from vane chord line in percent of airfoil chord]

(d) Double-Slotted Flap, Vane

Upper surface		Lower surface	
Station	Ordinate	Station	Ordinate
0	0	0	0
.42	.95	.42	-.93
.83	1.31	.83	-1.14
1.25	1.52	1.25	-1.20
1.67	1.67	1.67	-1.11
2.08	1.72	2.08	-.85
2.92	1.74	2.92	-.36
3.75	1.64	3.75	-.02
4.58	1.43	4.58	.18
5.42	1.13	5.42	.27
6.25	.75	6.25	.25
7.08	.28	7.08	.11
7.50	0	7.50	0
L.E. radius: 1.20 (center on vane chord line)			

TABLE II.- SUMMARY OF MAXIMUM-LIFT CHARACTERISTICS FOR THE NACA 64A010 AIRFOIL WITH VARIOUS HIGH-LIFT DEVICES. $R = 6 \times 10^6$

Model configuration	$c_{l_{max}}$	$\alpha_{c_{l_{max}}}$ deg	$\Delta c_{l_{max}}$	$\Delta\alpha_{c_{l_{max}}}$ deg
Plain airfoil[a]	1.10	11.0	---	---
Airfoil with split flap[a]	1.88	5.3	0.78[b]	-5.7[b]
Airfoil with double-slotted flap[a]	2.36	0.7	1.26[c]	-10.3[c]
Airfoil with leading-edge flap ($\delta_n = 30^\circ$)	1.66	18.8	0.56[d]	7.8[d]
Airfoil with leading-edge flap and split flap	2.58	15.8	0.70[d]	10.5[d]
			0.92[b]	-3.0[b]
Airfoil with leading-edge flap and double-slotted flap	3.09	10.5	0.73[d]	9.8[d]
			1.43[c]	-8.3[c]
Airfoil with leading-edge slat	1.94	22.0	0.84[e]	11.0[e]
Airfoil with leading-edge slat and split flap	2.81	18.2	0.93[e]	12.9[e]
			0.87[b]	-3.8[b]
Airfoil with leading-edge slat and double-slotted flap	3.08	10.8	0.72[e]	10.1[e]
			1.14[c]	-11.2[c]

[a]Data from figure 4(a), $\delta_n = 0^\circ$
[b]Increments produced by split flap
[c]Increments produced by double-slotted flap
[d]Increments produced by leading-edge flap
[e]Increments produced by leading-edge slat

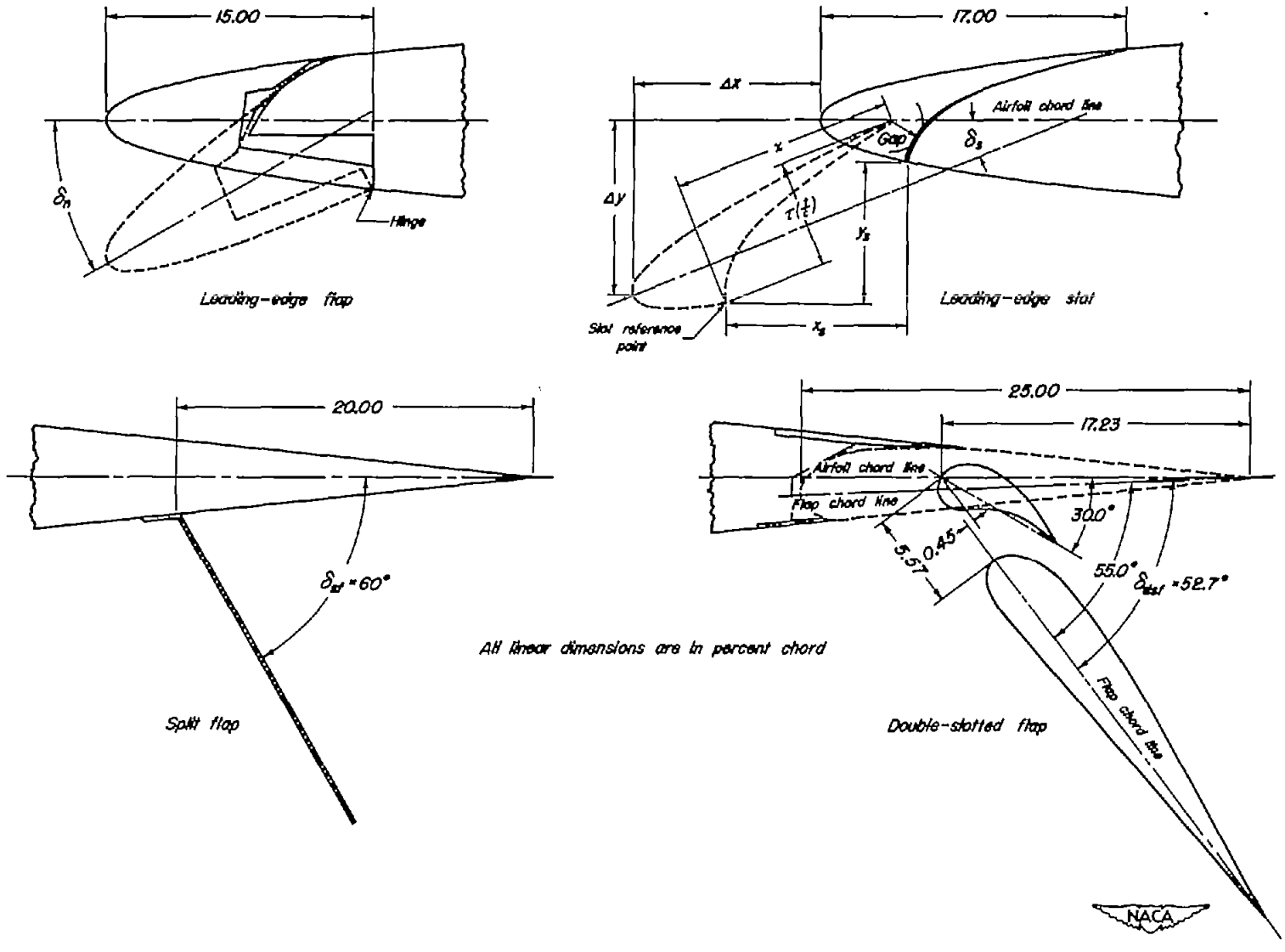

Figure 1.- Geometry and reference dimensions for the various high-lift devices.

(a) Model with leading-edge slat and split flap.

(b) Model with leading-edge flap and no trailing-edge flap.

Figure 2.- Photographs of NACA 64A010 airfoil mounted in test section of the Ames 7- by 10-foot wind tunnel No. 1.

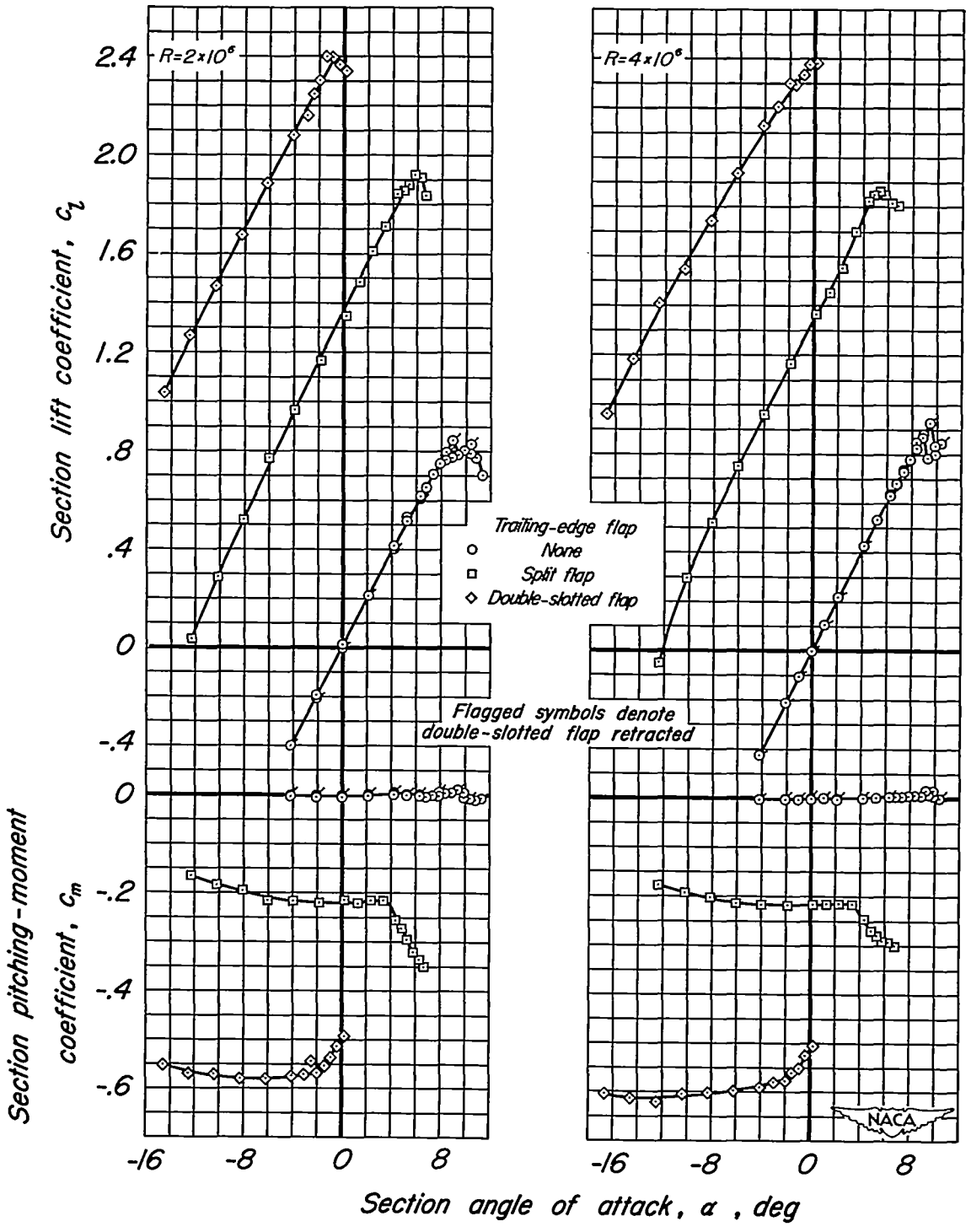

(a) R = 2 and 4 x 10^6.

Figure 3.- Section lift and pitching-moment characteristics for the model with the leading-edge slat retracted.

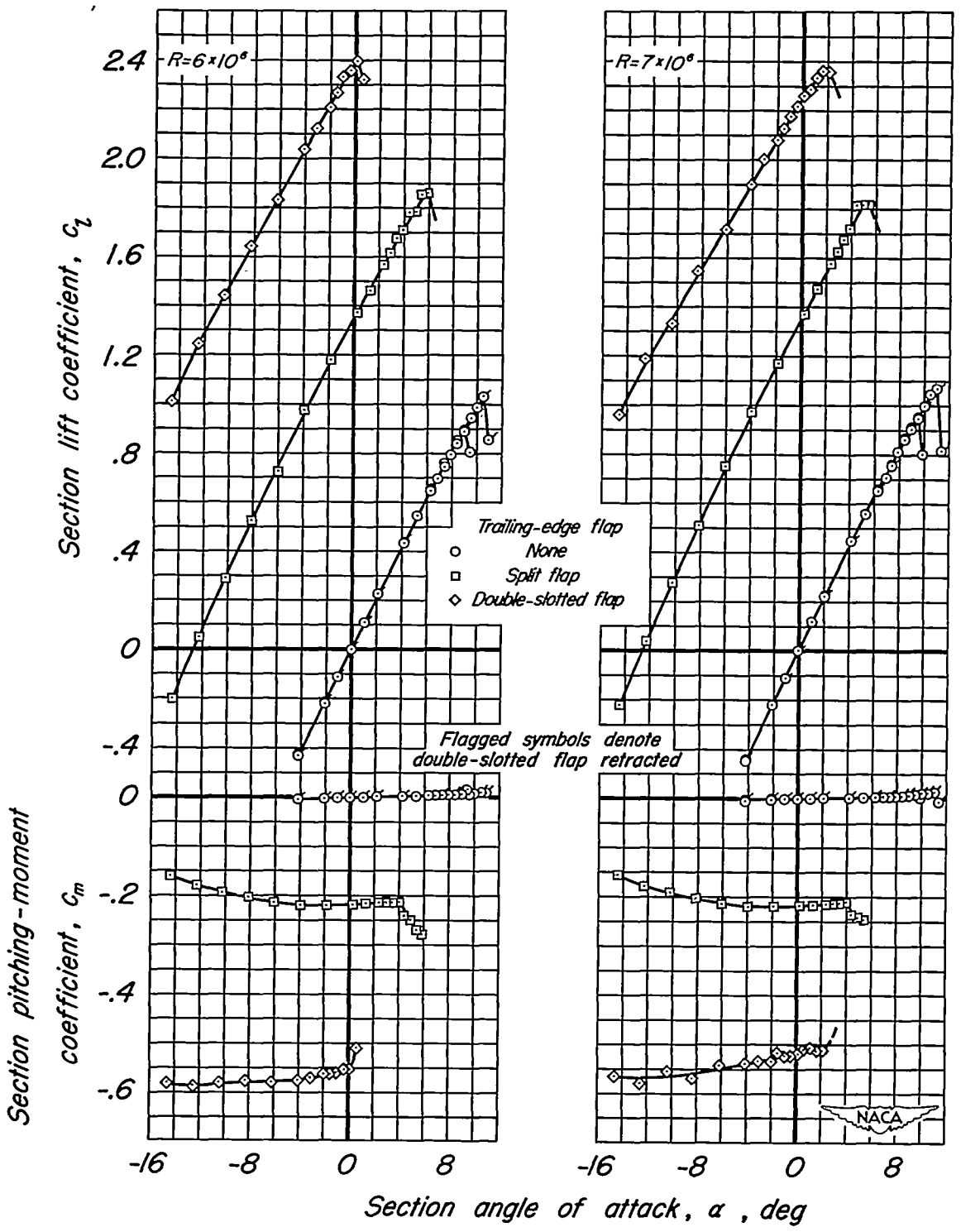

(b) R = 6 and 7 × 10^6.

Figure 3.- Concluded.

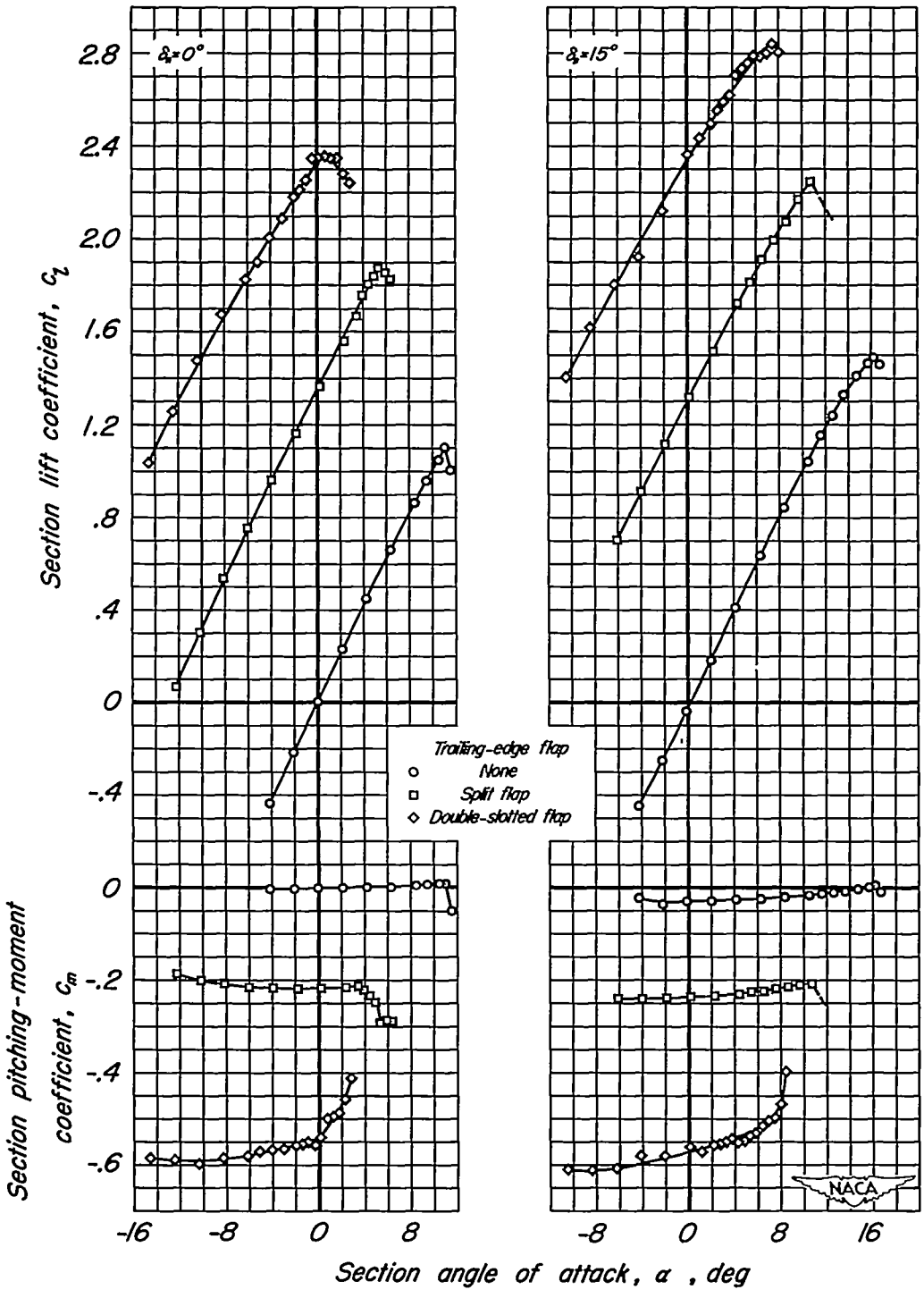

(a) $\delta_n = 0^\circ$ and 15°.

Figure 4.- Section lift and pitching-moment characteristics for the model with the leading-edge flap. $R = 6 \times 10^6$.

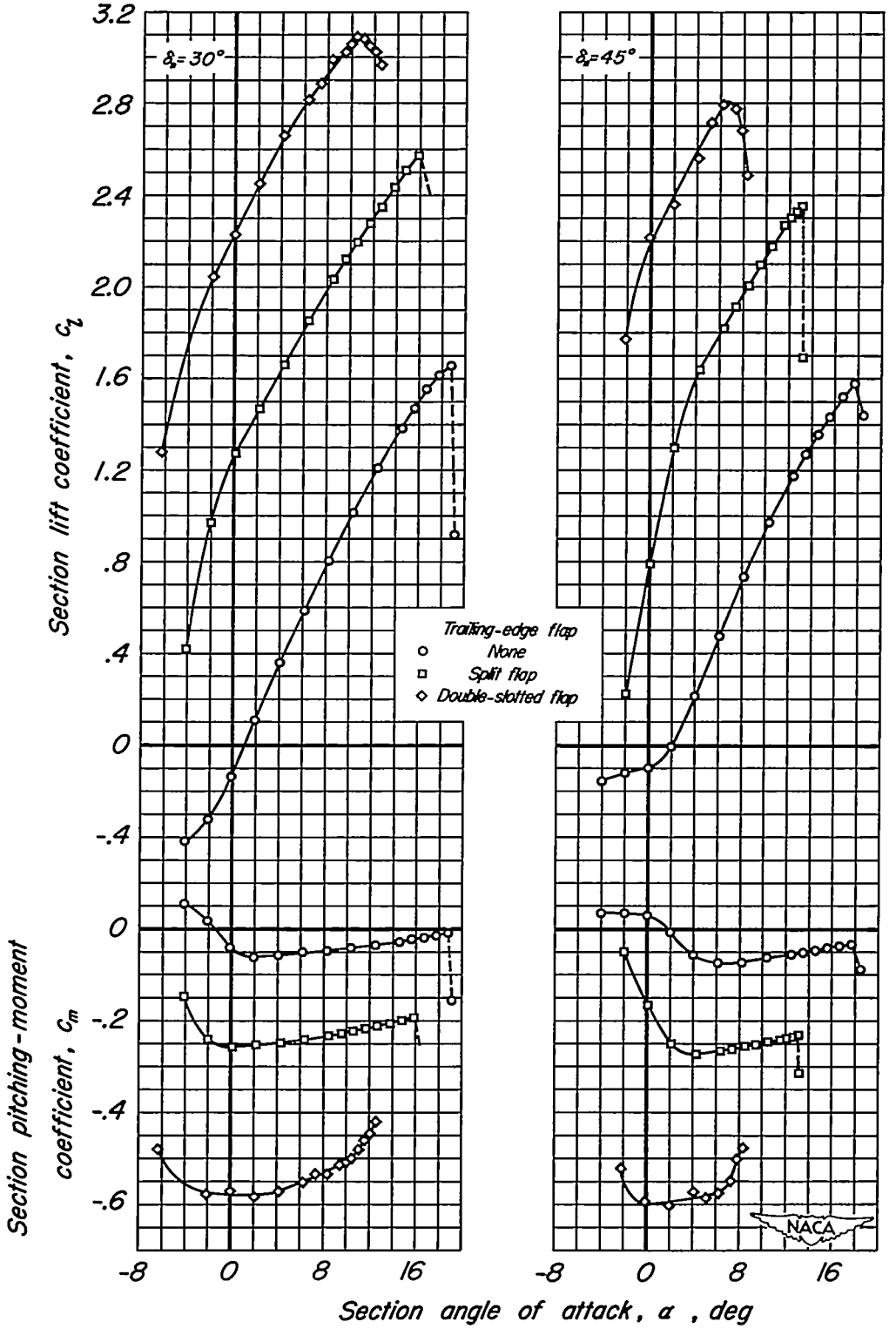

(b) δ_n = 30° and 45°.

Figure 4.- Concluded.

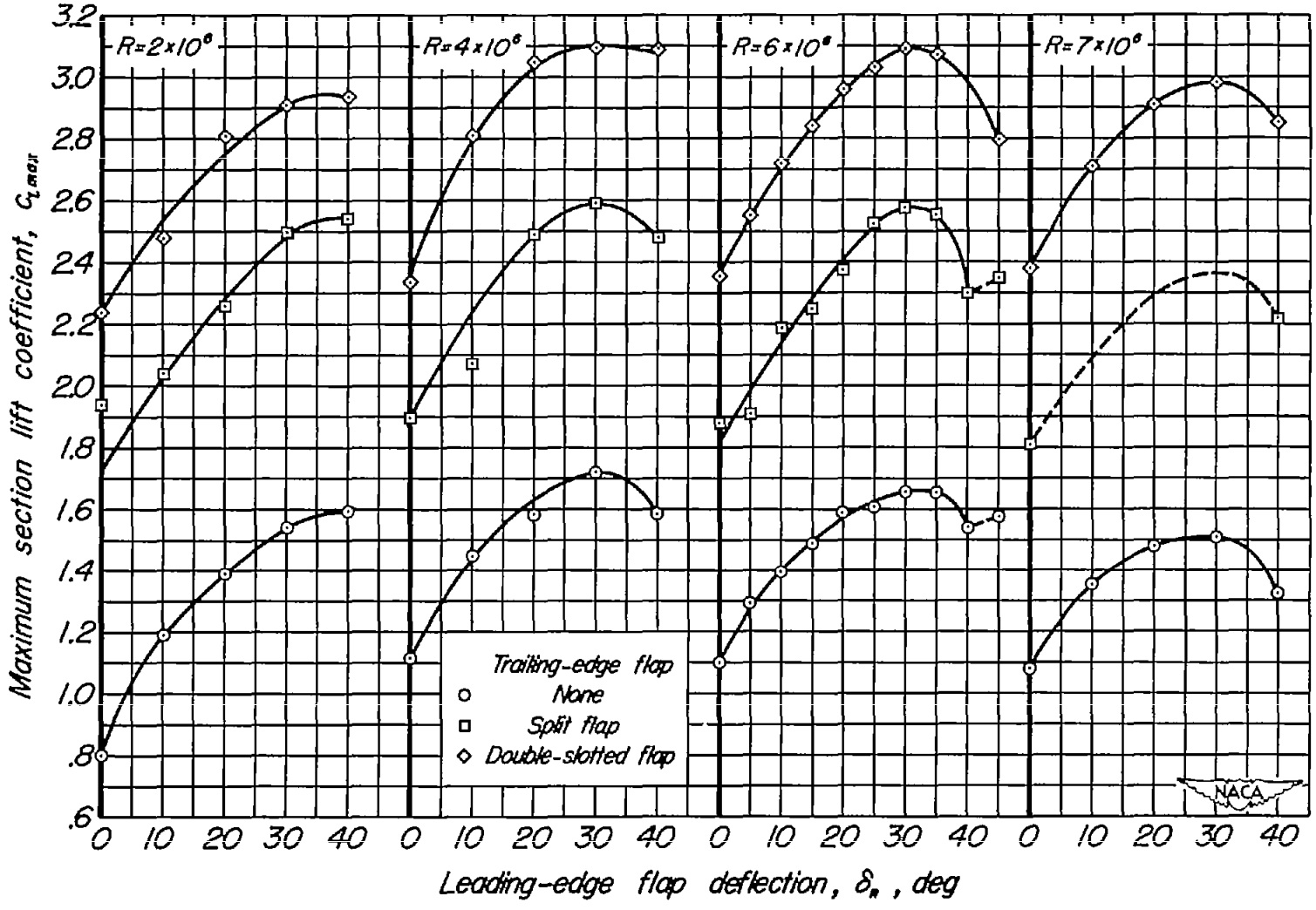

Figure 5.- Variation of maximum section lift coefficient with leading-edge-flap deflection.

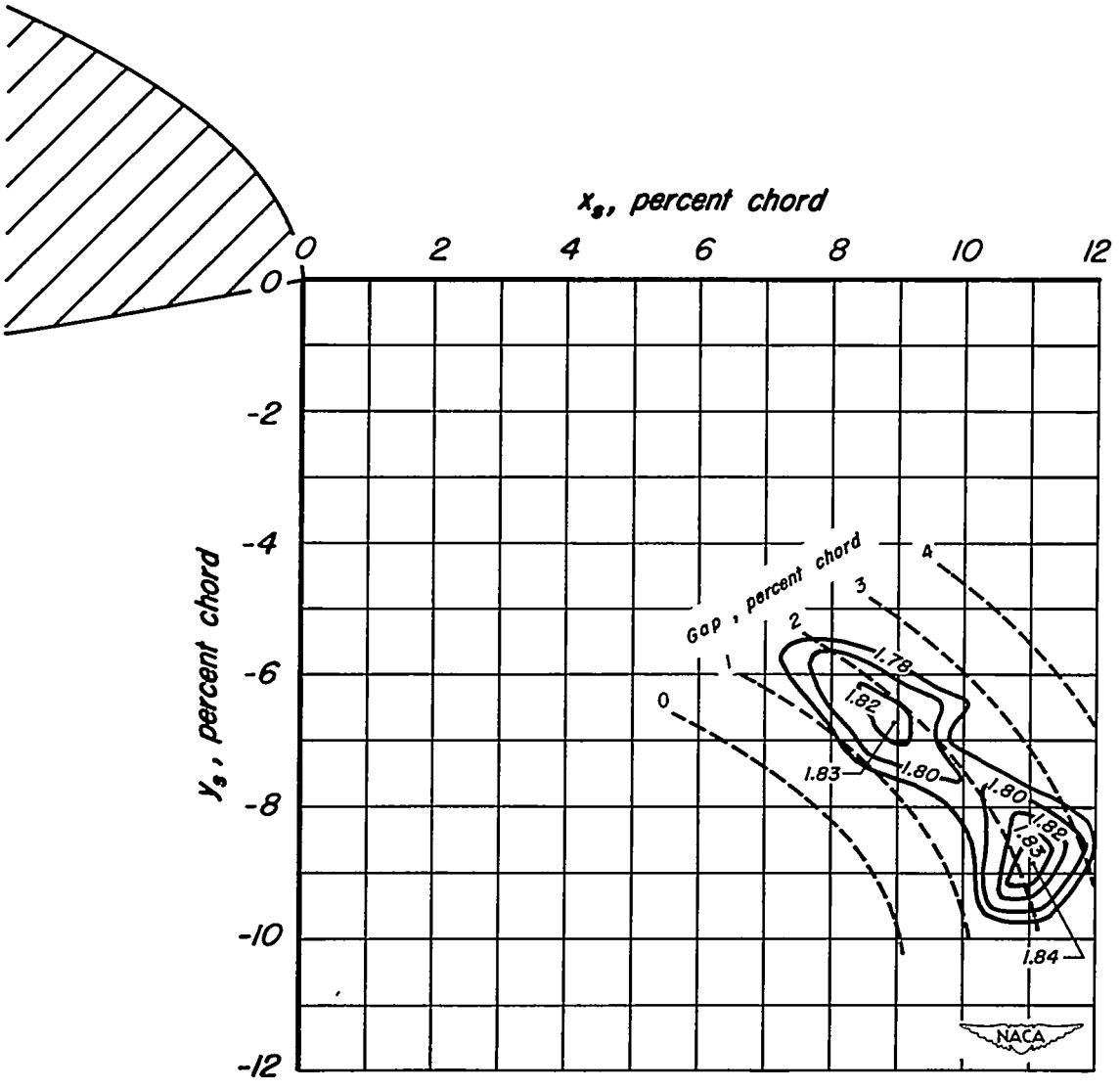

(a) $\delta_s = 21.6°$.

Figure 6.- Contours of maximum section lift coefficient for various positions of the slat reference point on the model with no trailing-edge flap. $R = 6 \times 10^6$.

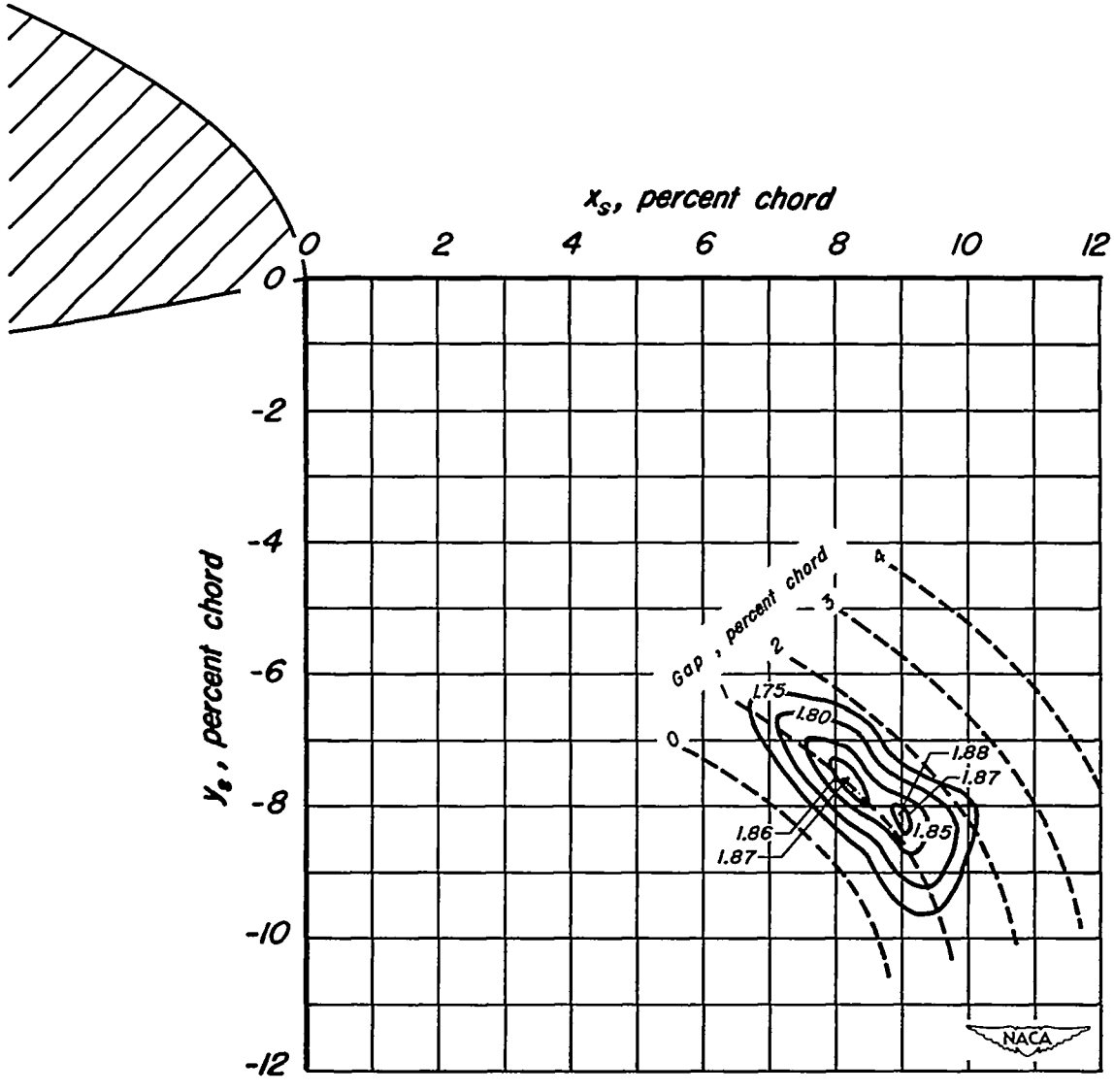

(b) $\delta_s = 23.6°$.

Figure 6.- Continued.

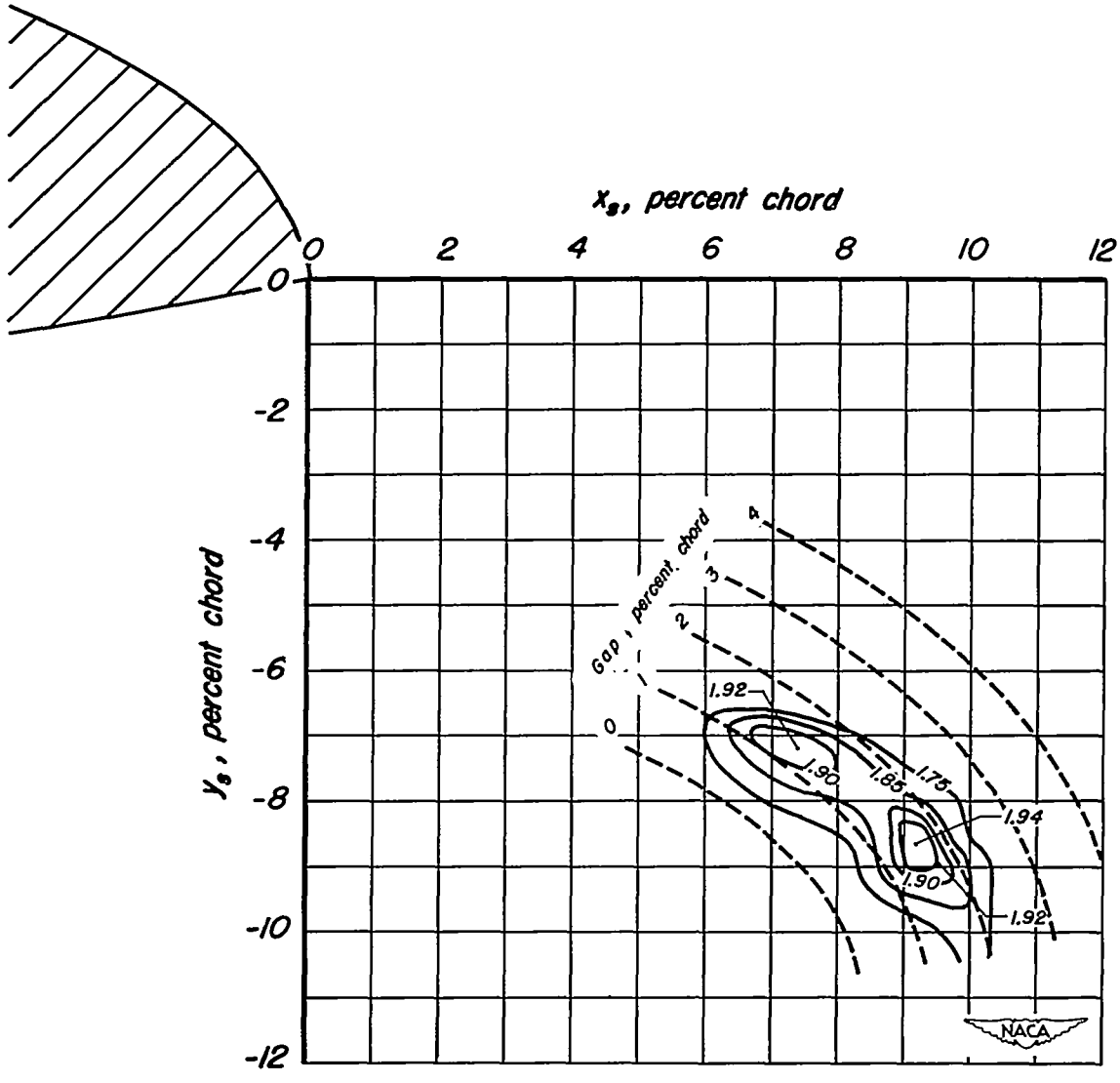

(c) $\delta_s = 25.6°$.

Figure 6.- Continued.

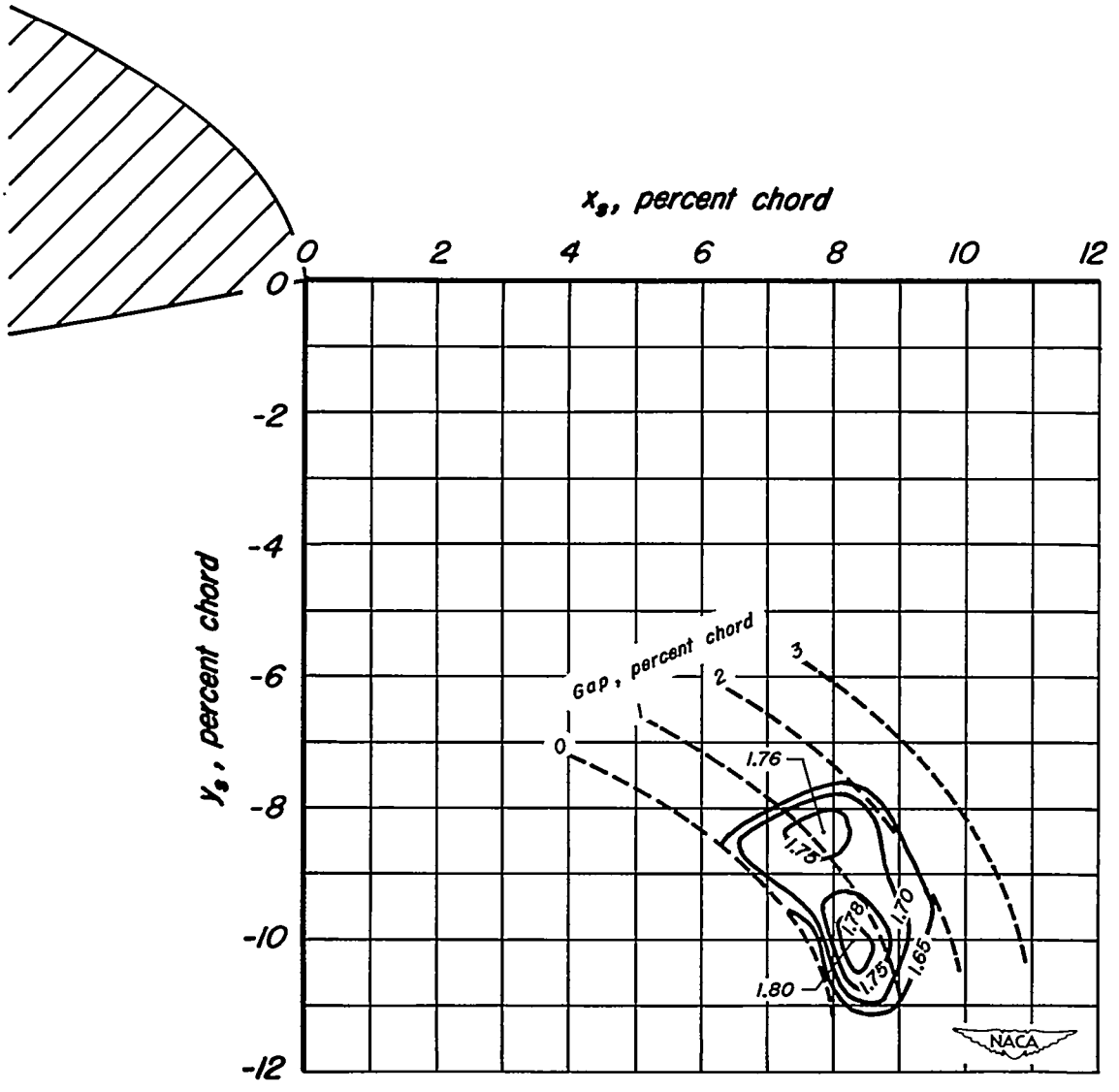

(d) $\delta_s = 27.6°$.

Figure 6.- Concluded.

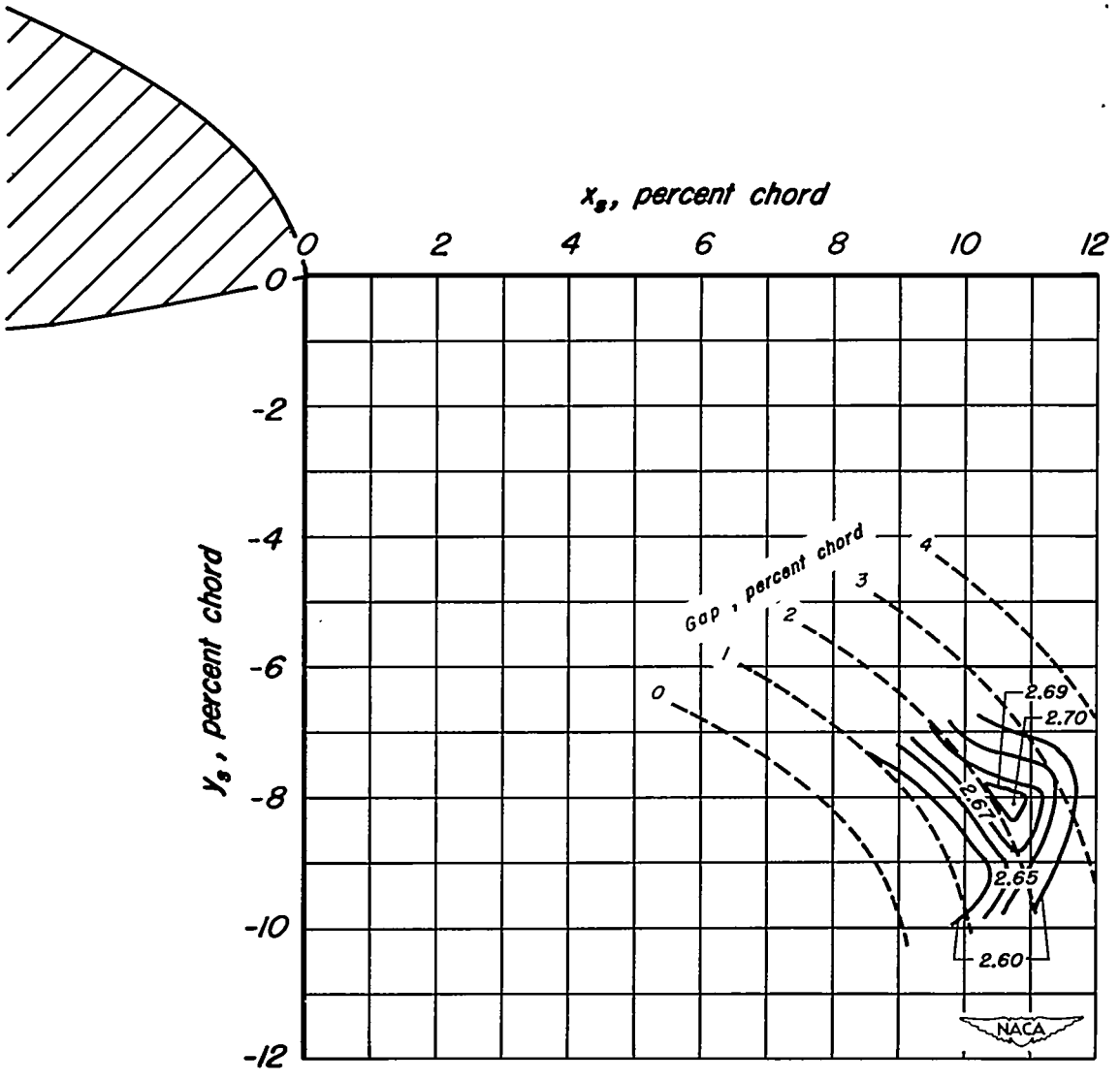

(a) $\delta_s = 21.6°$.

Figure 7.- Contours of maximum section lift coefficient for various positions of the slat reference point on the model with the split flap. $R = 6 \times 10^6$.

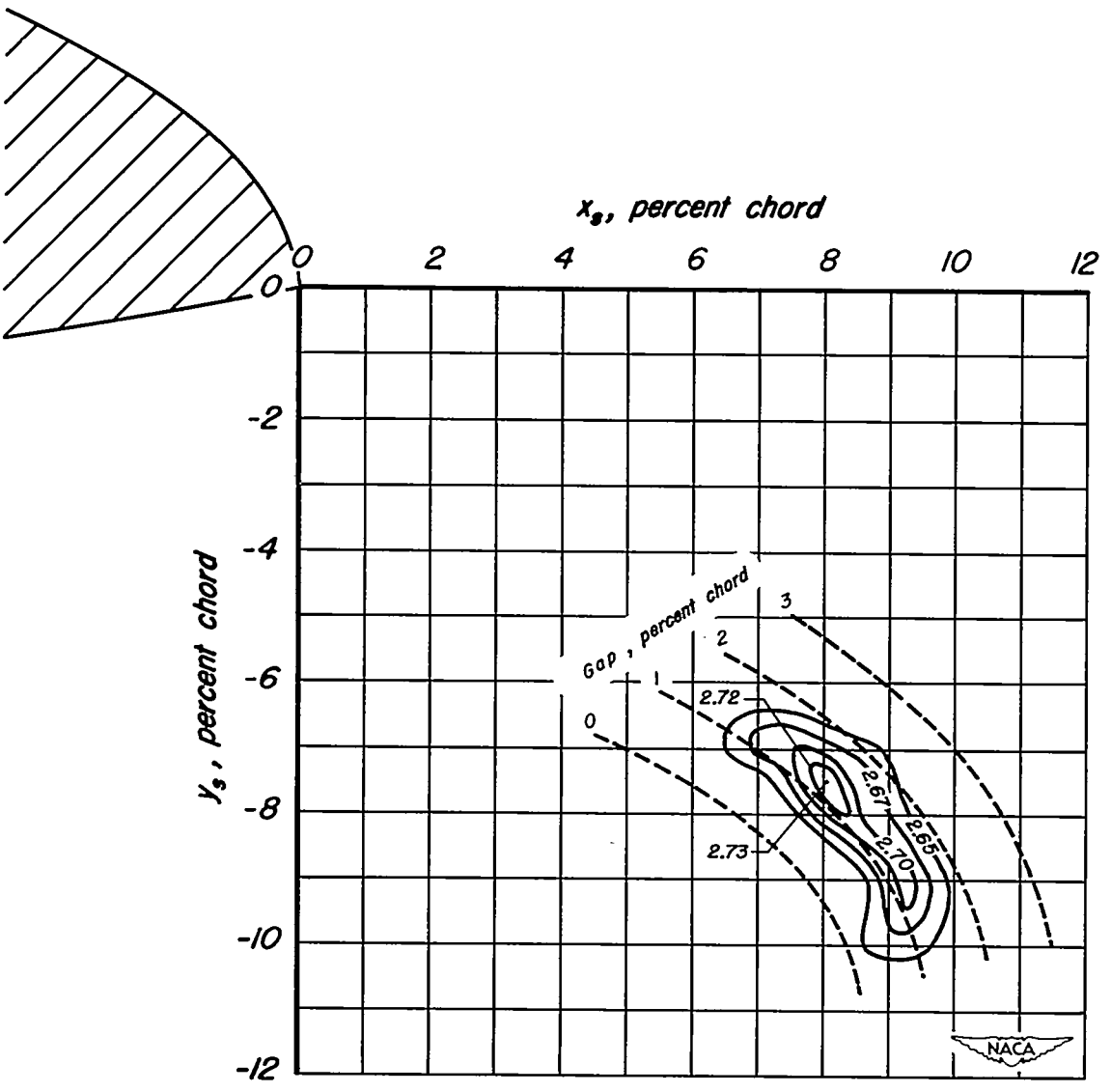

(b) $\delta_s = 24.6°$.

Figure 7.- Continued.

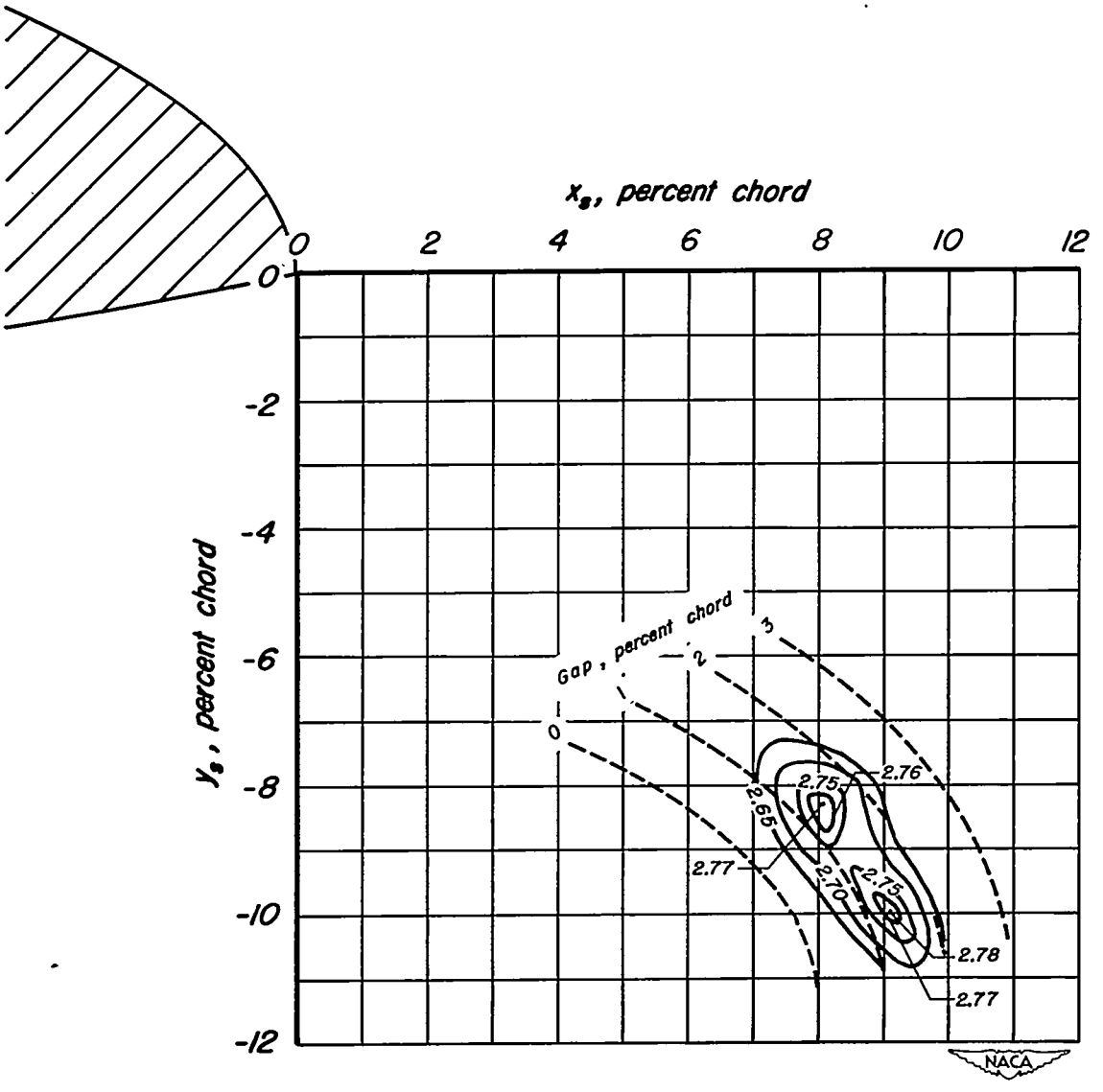

(c) $\delta_s = 27.6°$.

Figure 7.- Continued.

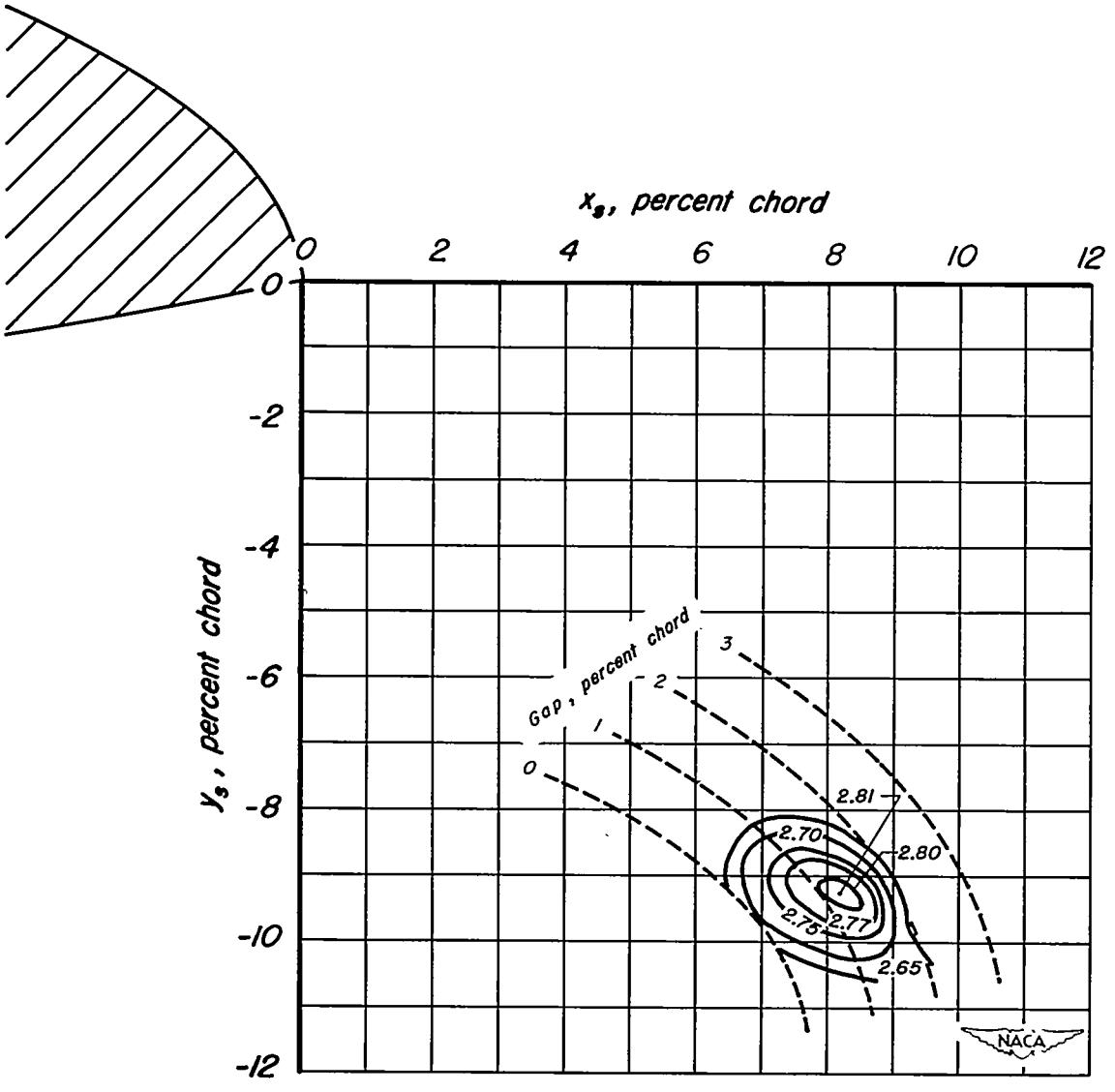

(d) $\delta_s = 29.1°$.

Figure 7.- Continued.

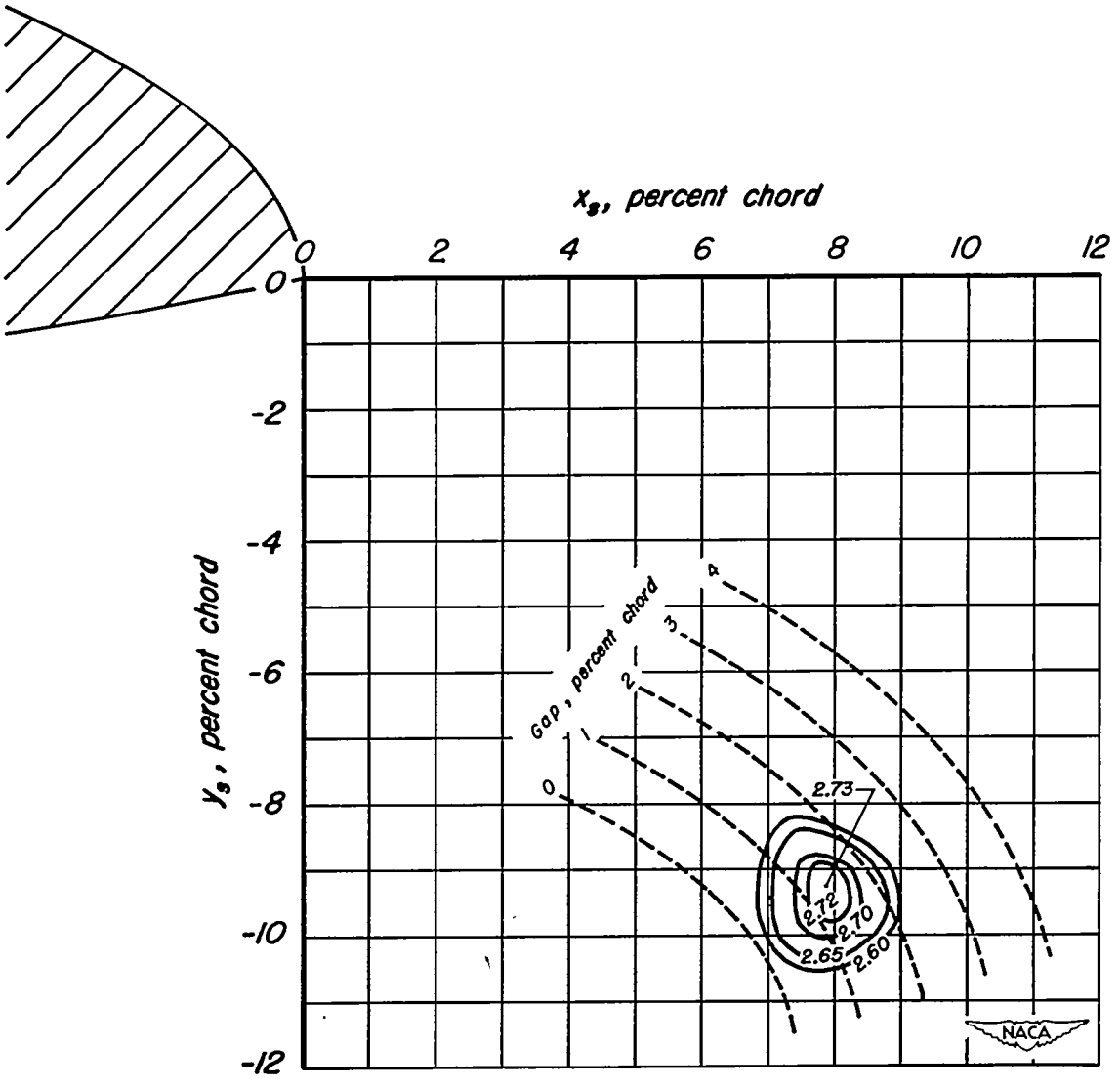

(e) $\delta_e = 30.6^\circ$.

Figure 7.- Concluded.

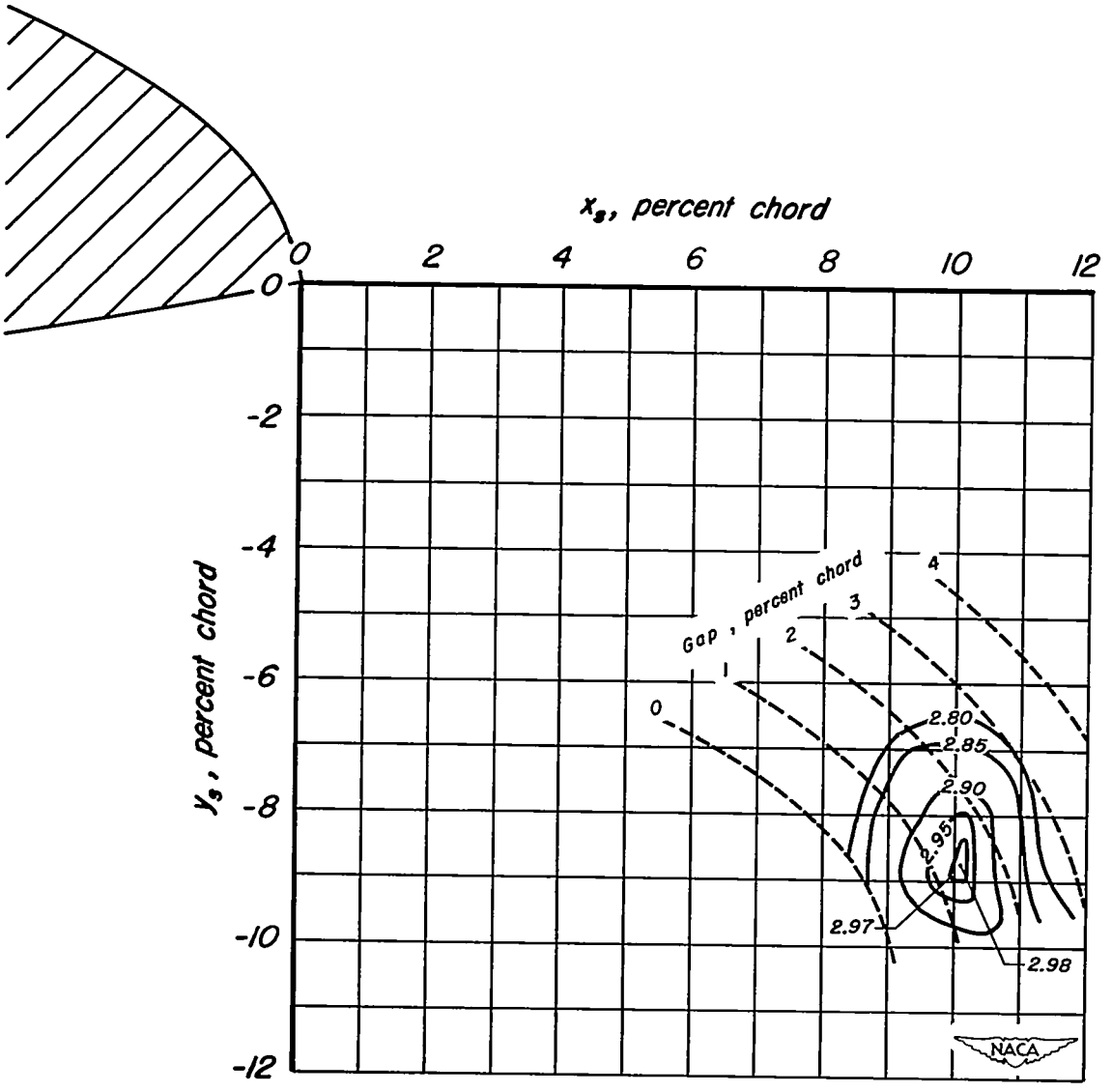

(a) $\delta_s = 21.6^\circ$.

Figure 8.- Contours of maximum section lift coefficient for various positions of the slat reference point on the model with the double-slotted flap. $R = 6 \times 10^6$.

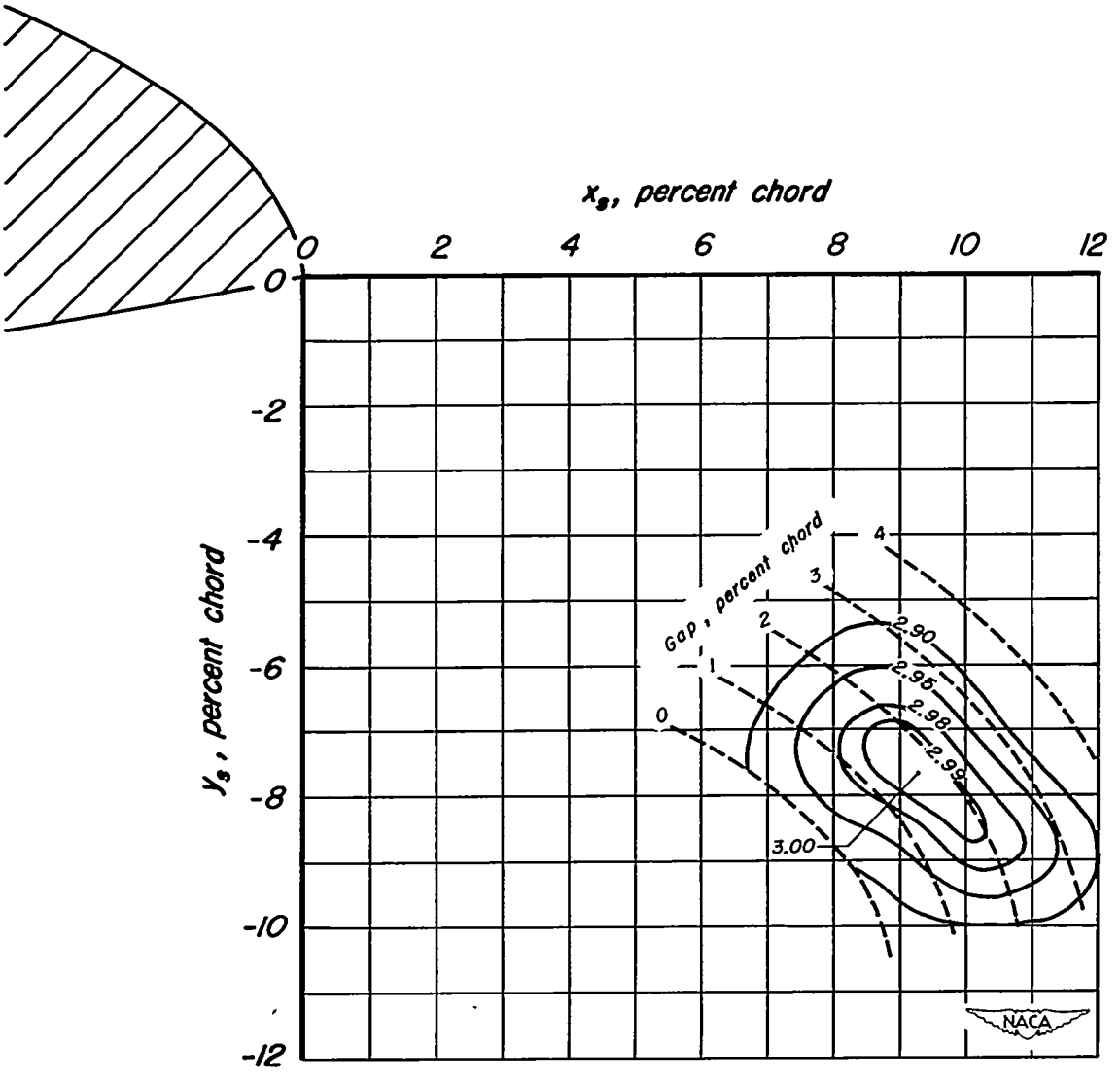

(b) $\delta_s = 23.1^\circ$.

Figure 8.- Continued.

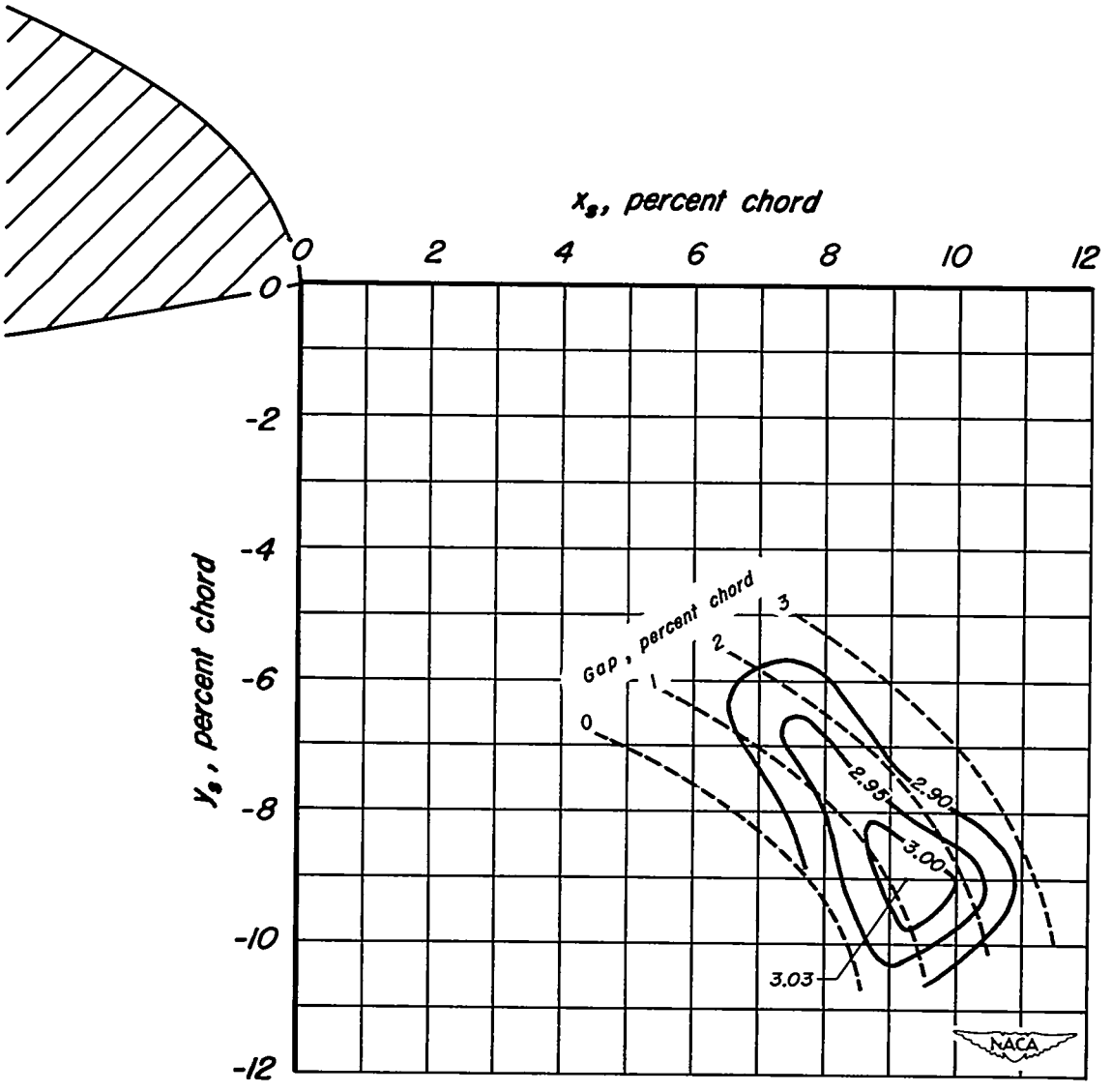

(c) $\delta_s = 24.6°$.

Figure 8.- Continued.

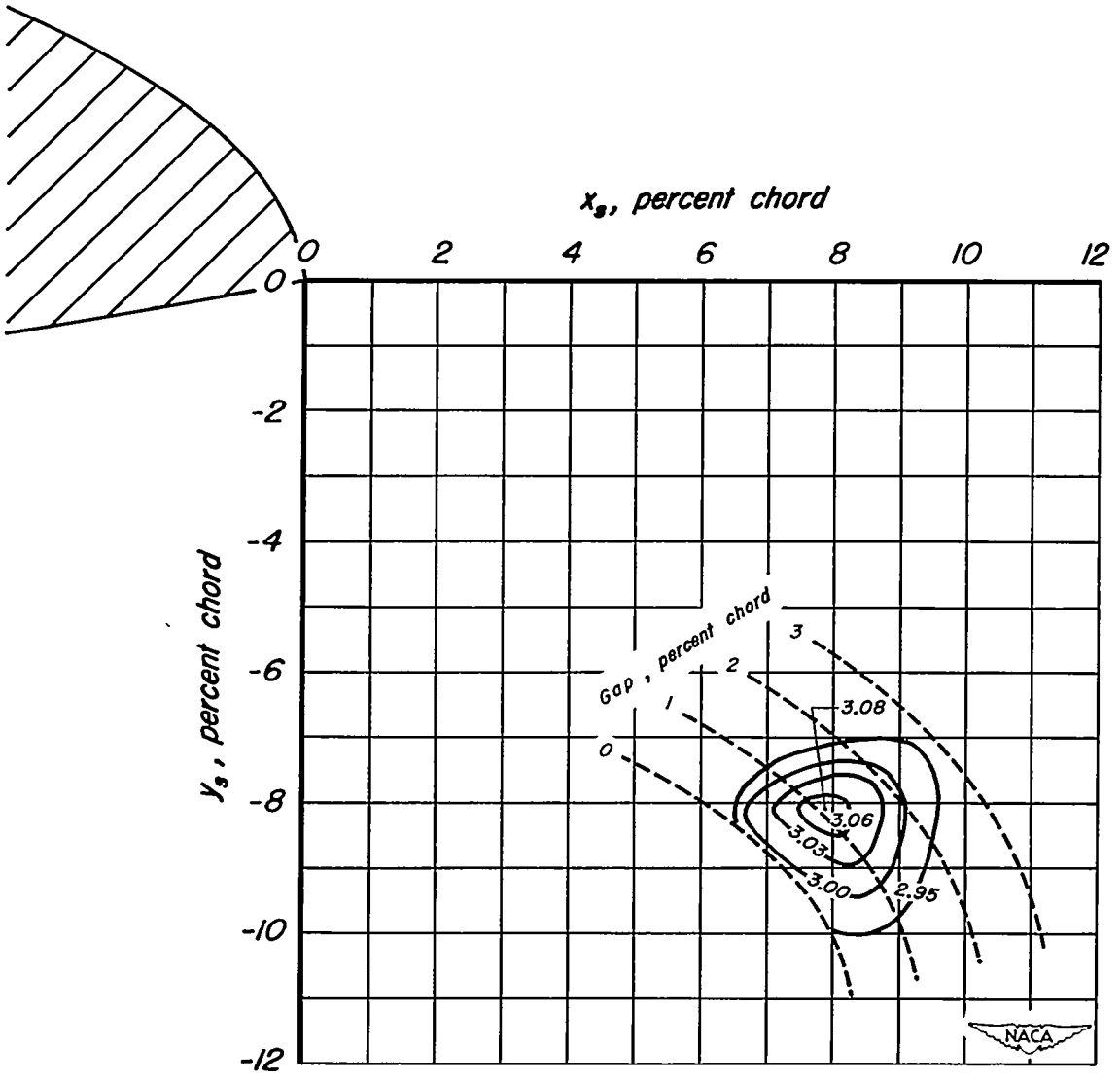

(d) $\delta_s = 26.1^\circ$.

Figure 8.- Continued.

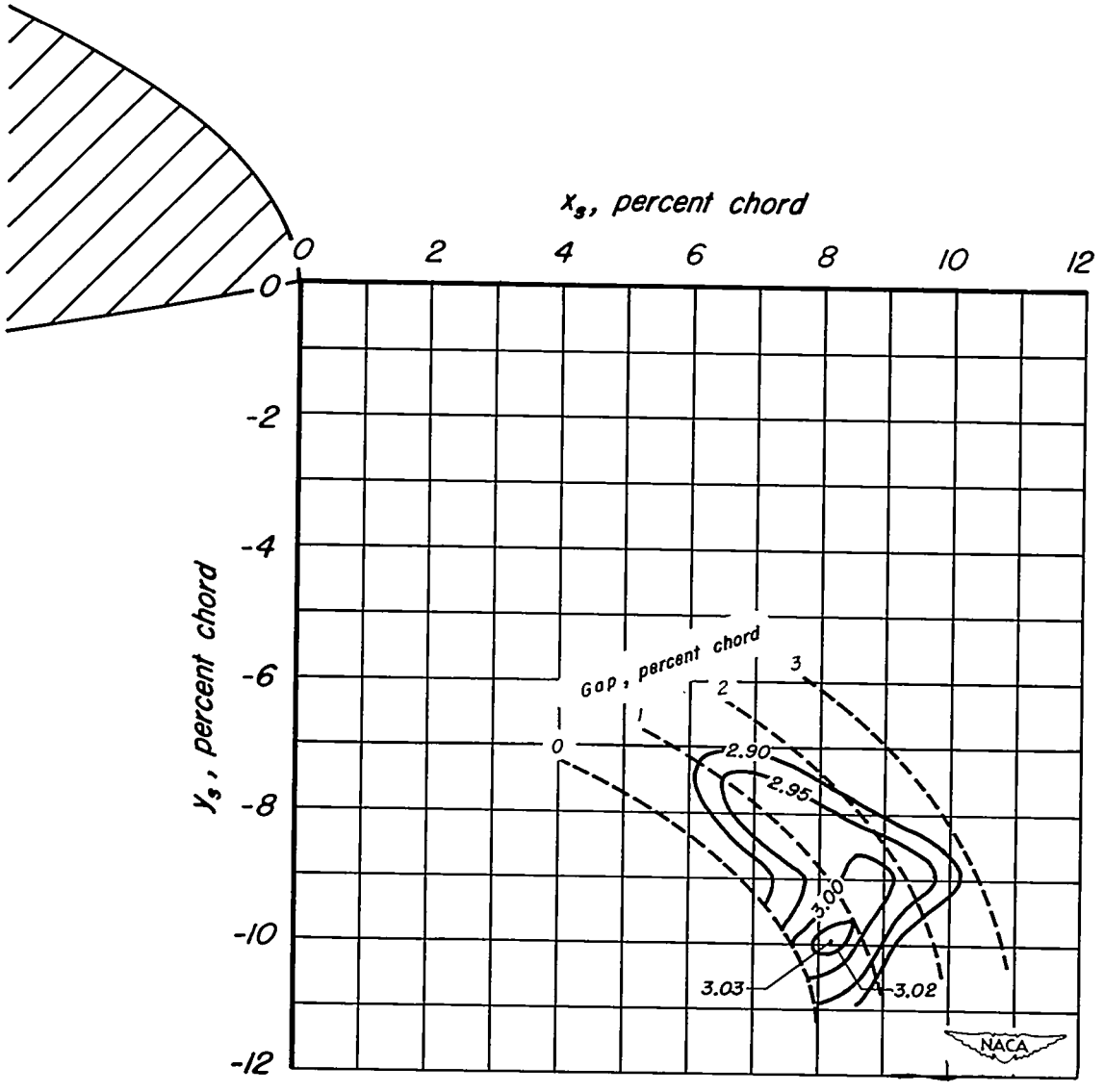

(e) $\delta_s = 27.6^\circ$.

Figure 8.- Concluded.

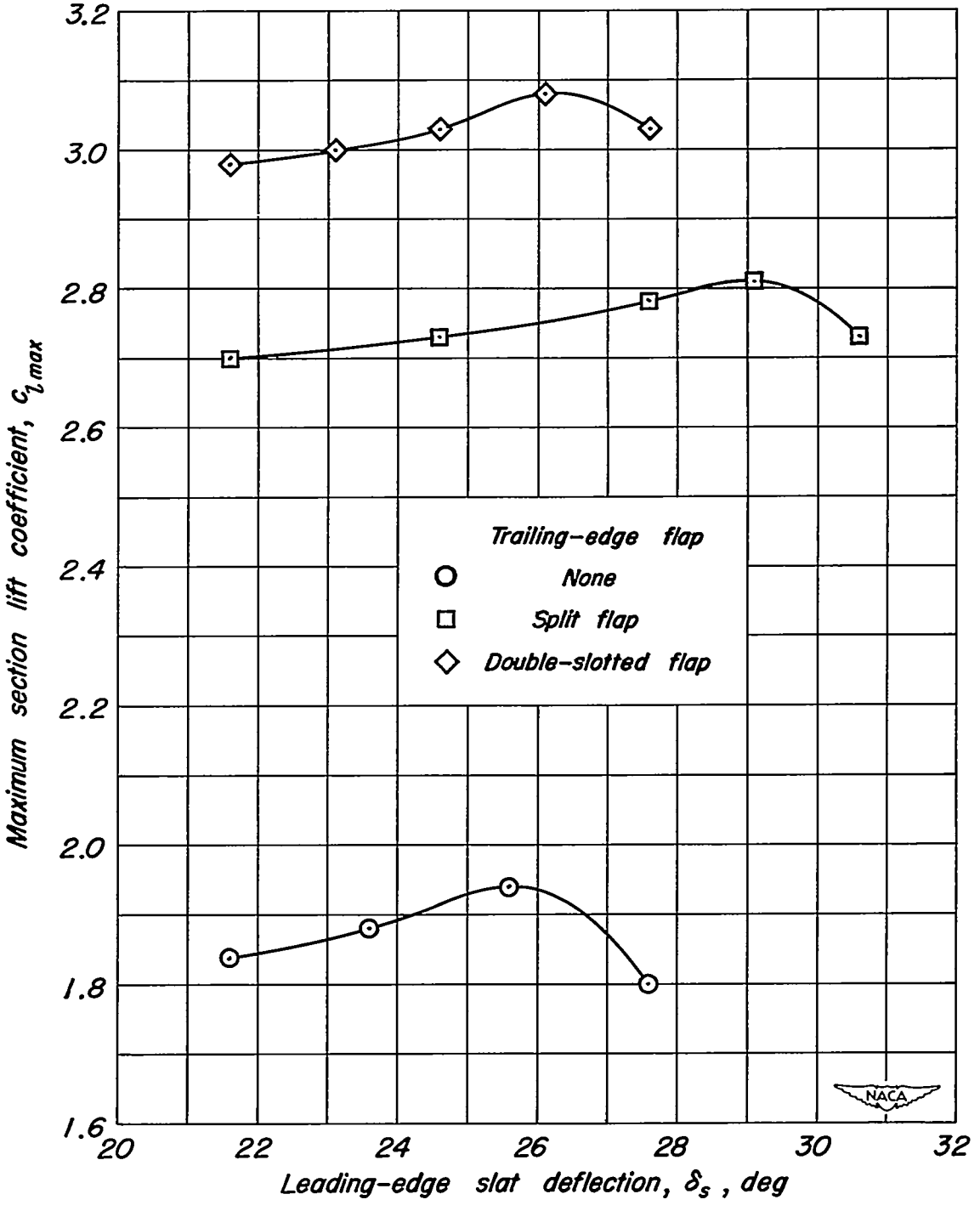

Figure 9.- Variation of maximum section lift coefficient with leading-edge-slat deflection. $R = 6 \times 10^6$.

Sym.	Airfoil	Trailing-edge flap	Reference
○	NACA 64A010	none	Present report
□	do.	Split flap deflected 60°	do.
◇	do.	Double-slotted flap deflected 52.7°	do.
△	NACA 64$_1$-212	none	4
▽	do.	Split flap deflected 60°	do.
▷	NACA 65A109	none	do.
◁	do.	Split flap deflected 60°	do.
⊿	NACA 23012	none	5
▷	do.	Split flap deflected 60°	do.
◁	do.	Single-slotted flap deflected 40°	do.

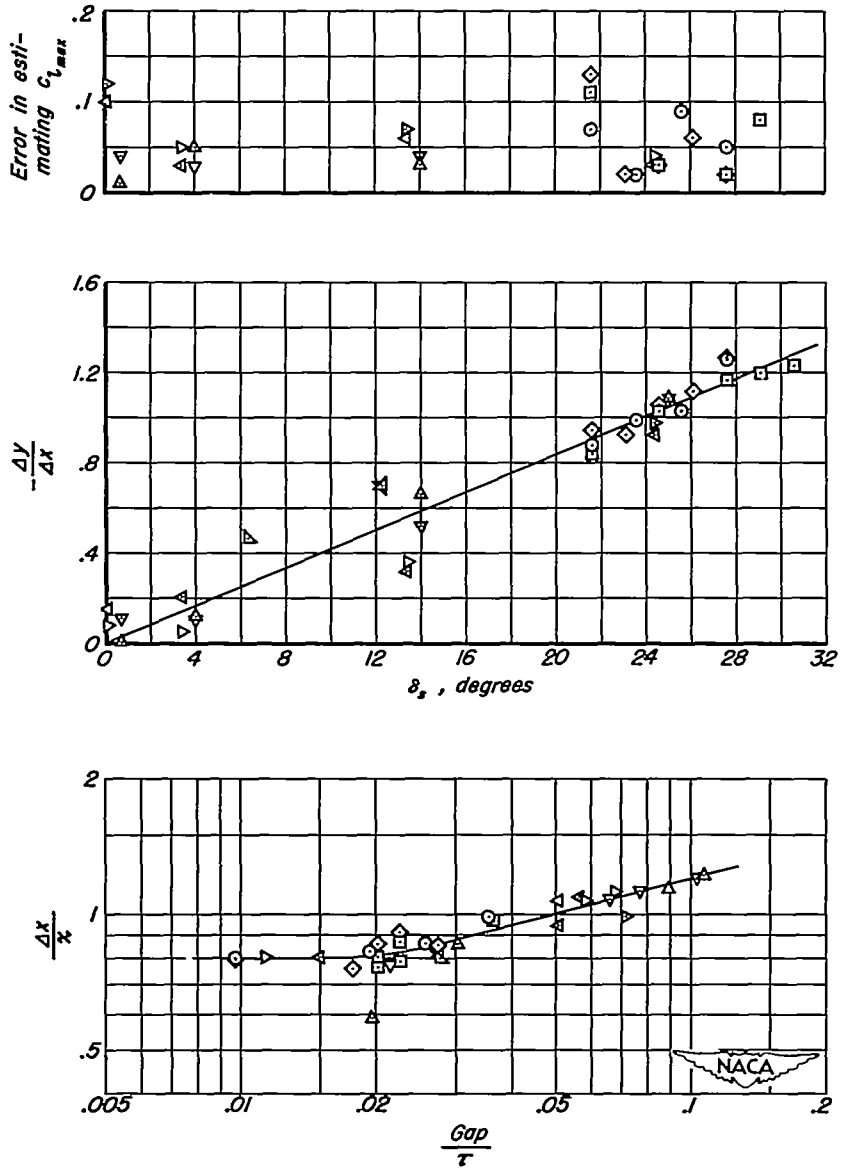

Figure 10.- Slat positions for largest maximum lift.

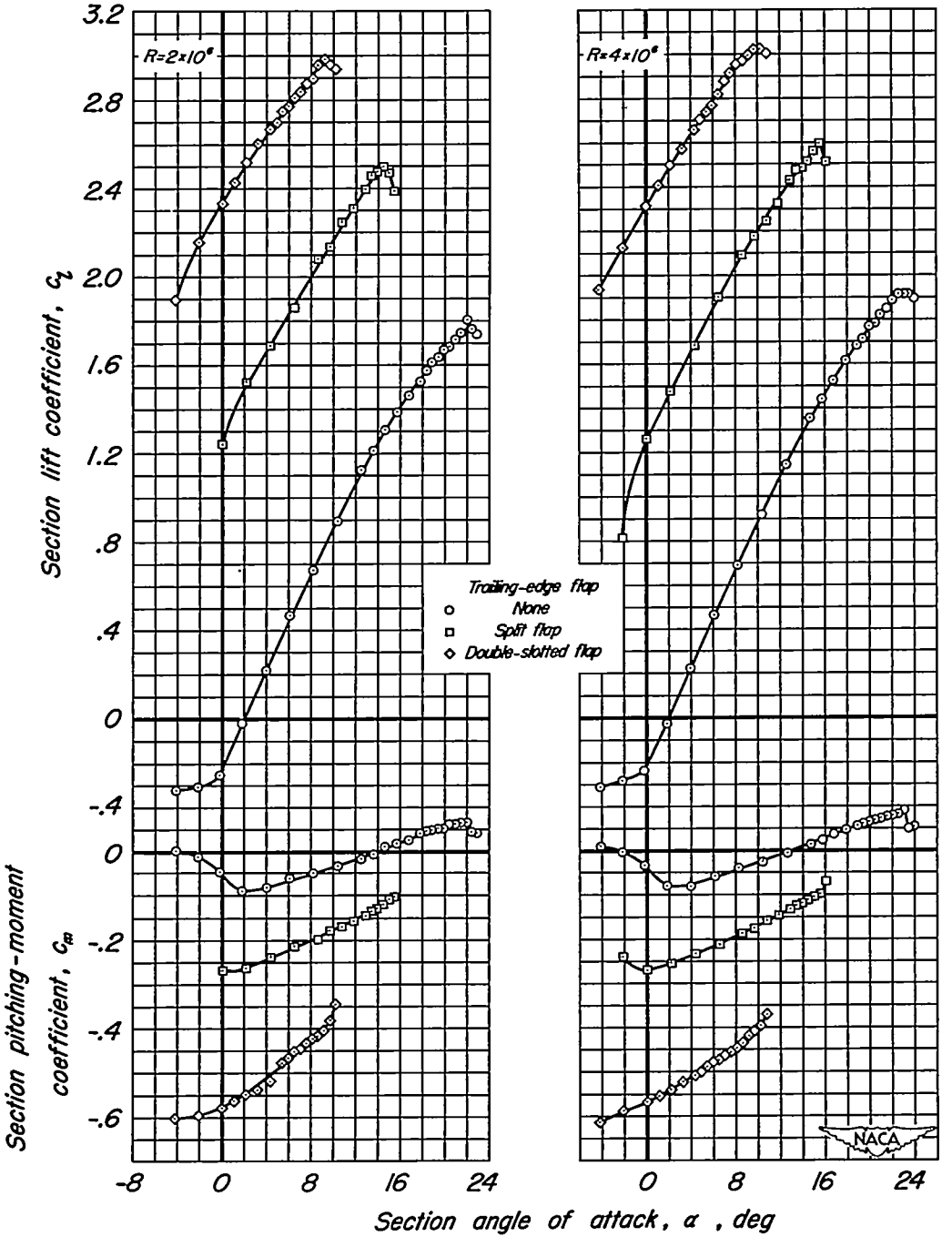

(a) R = 2 and 4 × 10^6.

Figure 11.- Section lift and pitching-moment characteristics for the model with the leading-edge slat extended. Slat in optimum position for model without a trailing-edge flap (δ_s = 25.6°, x_s = 0.092c, y_s = -0.087c, Gap = 0.0160c).

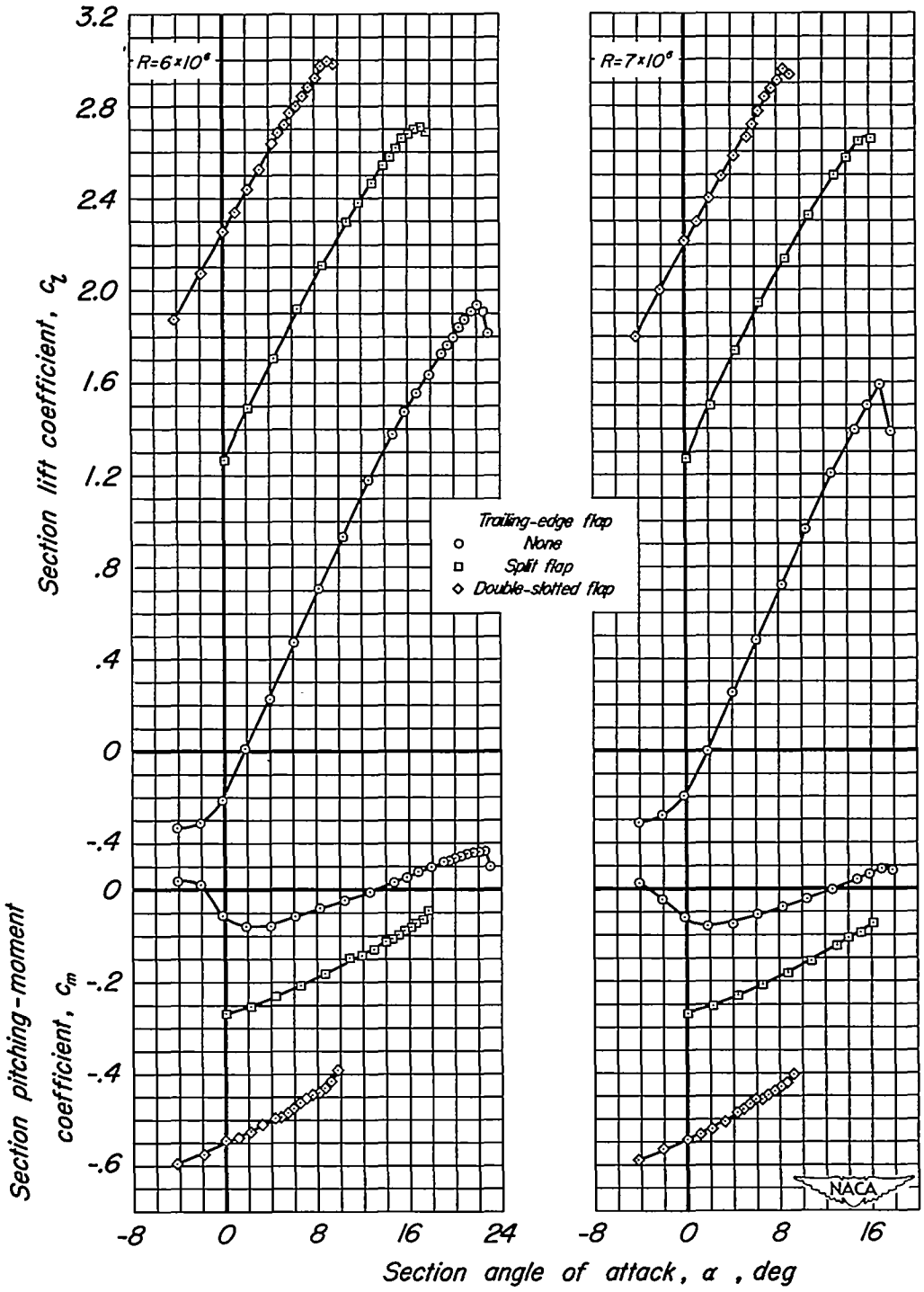

(b) R = 6 and 7 × 10^6.

Figure 11.- Concluded.

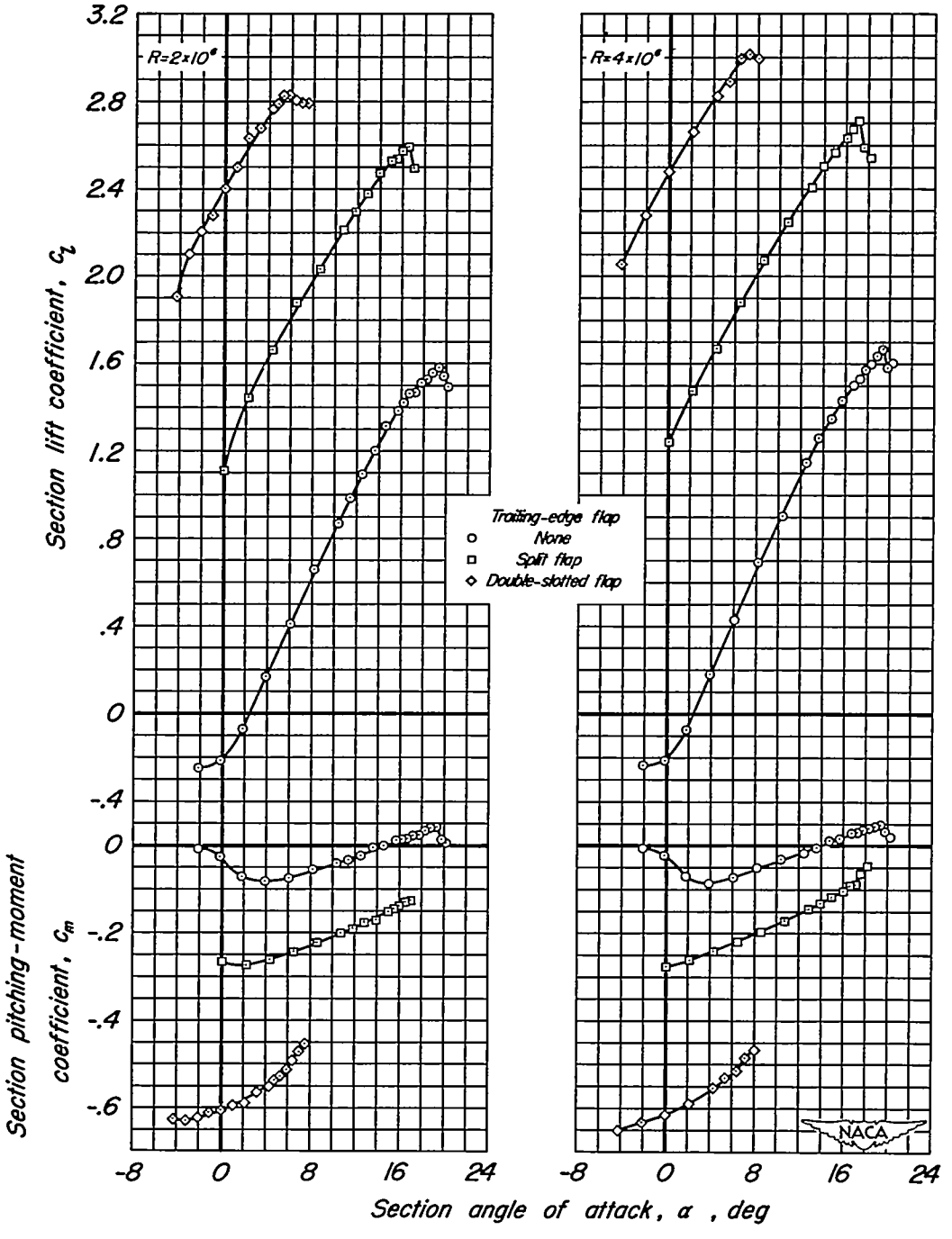

(a) R = 2 and 4 × 10^6.

Figure 12.- Section lift and pitching-moment characteristics for the model with the leading-edge slat extended. Slat in optimum position for model with the split flap deflected 60° (δ_s = 29.1°, x_s = 0.082c, y_s = -0.093c, Gap = 0.0125c).

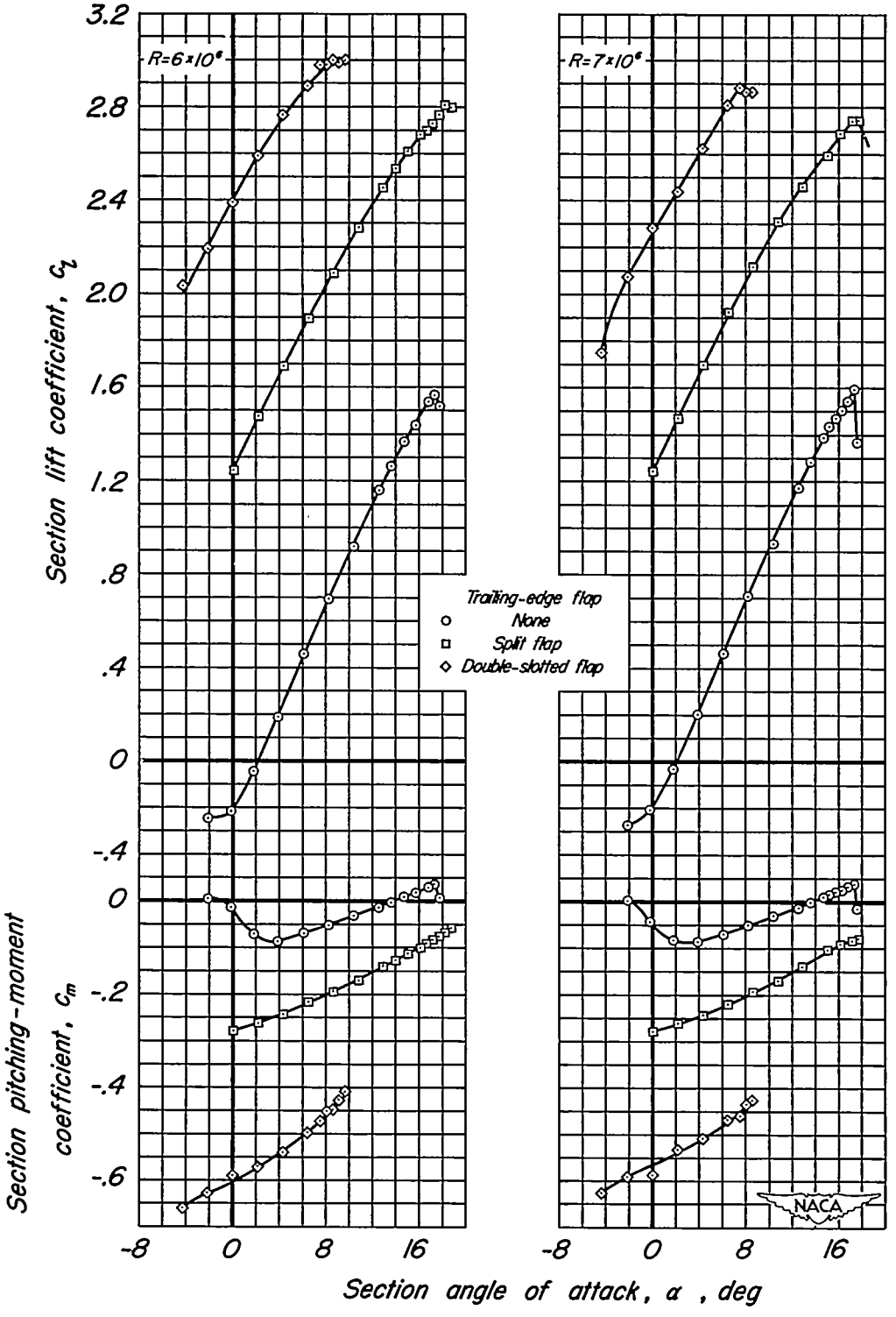

(b) R = 6 and 7 × 10^6.

Figure 12.- Concluded.

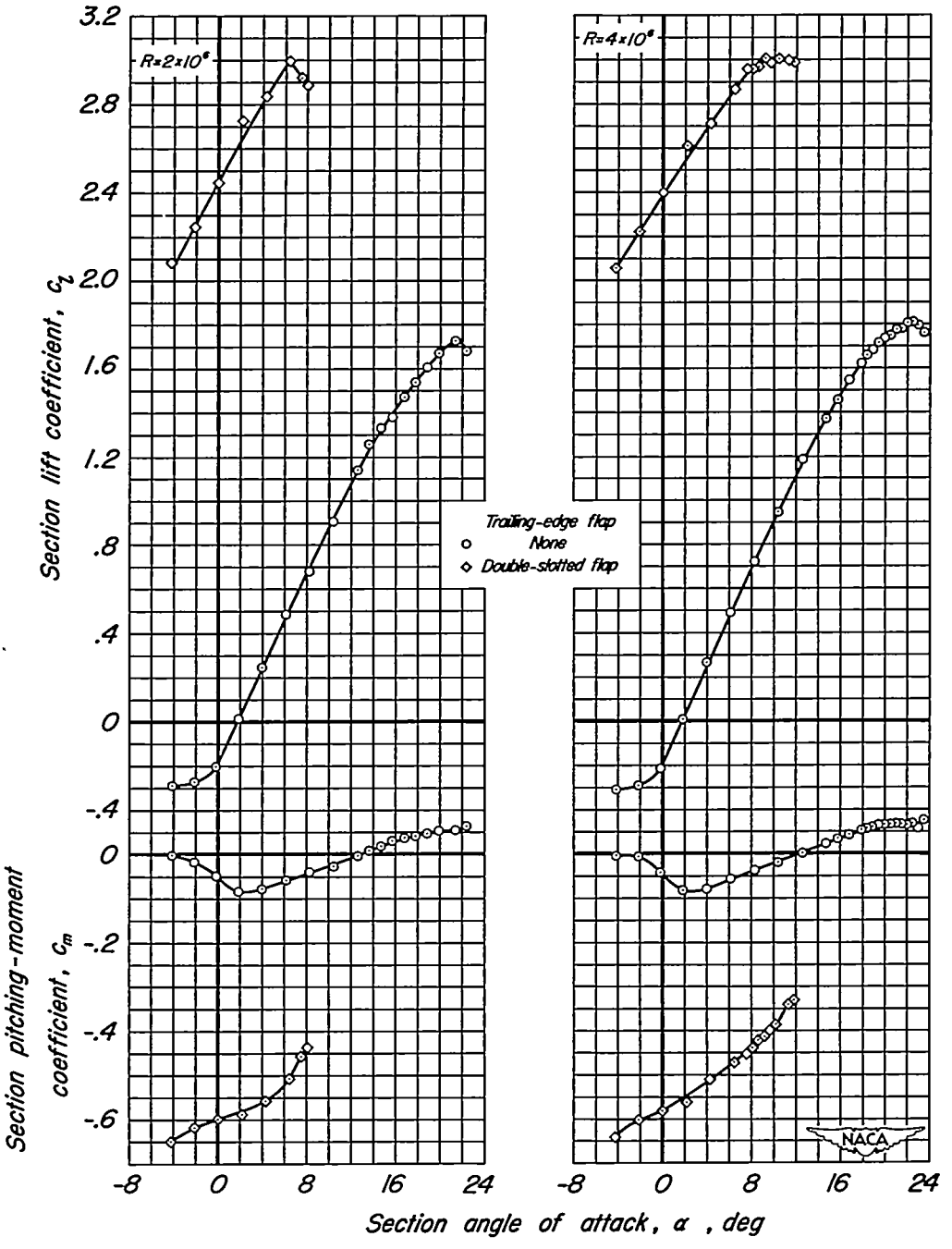

(a) R = 2 and 4 × 10^6.

Figure 13.- Section lift and pitching-moment characteristics for the models with the leading-edge slat extended. Slat in optimum position for model with the double-slotted flap deflected 52.7° (δ_s = 26.1°, x_s = 0.079c, y_s = -0.081c, Gap = 0.011Oc).

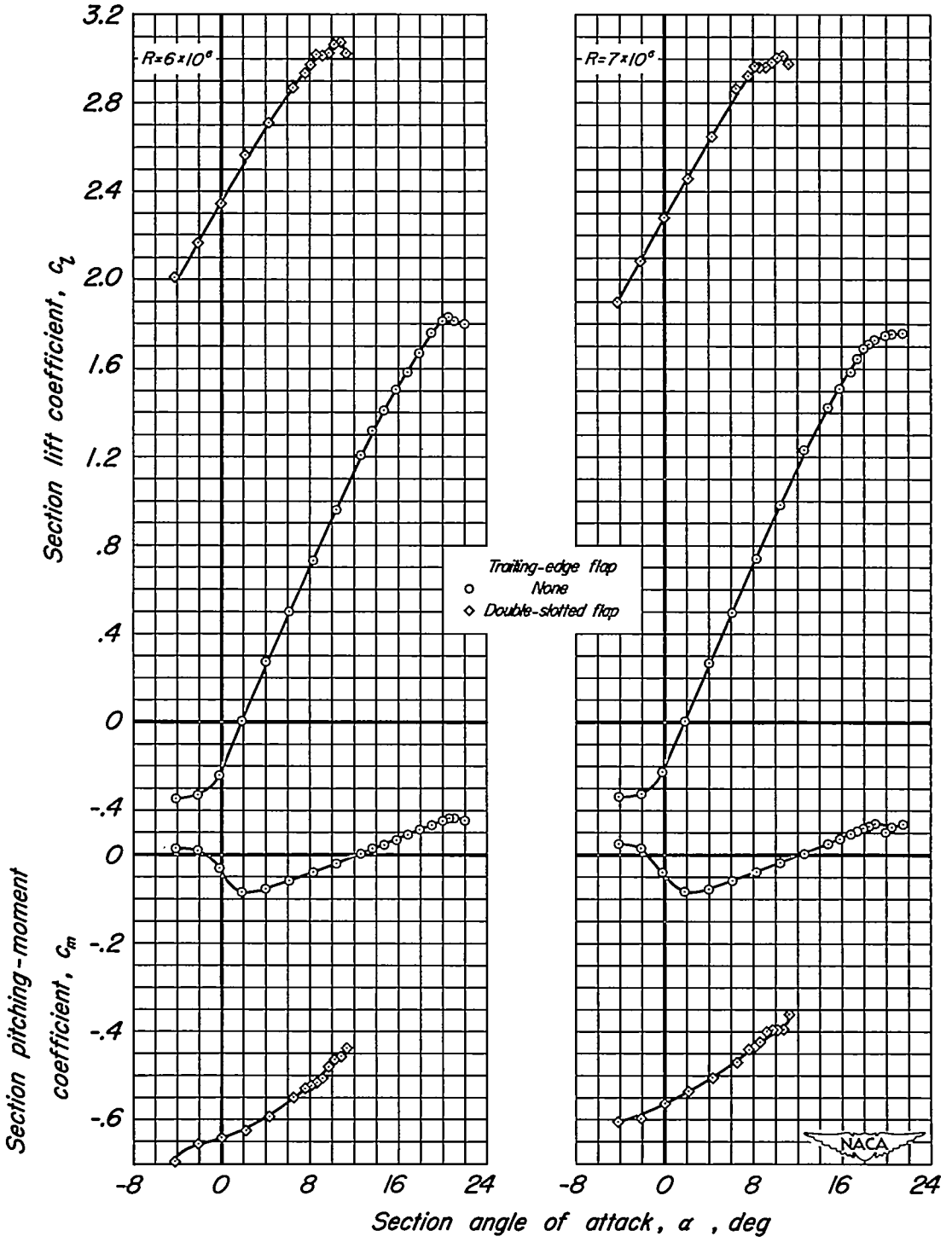

(b) R = 6 and 7 × 10^6.

Figure 13.- Concluded.

NACA-Langley - 9-14-53 - 1000